The Thesis Committee for Gail Ruth Gutowski
Certifies that this is the approved version of the following thesis:

Effect of modeled pre-industrial Greenland Ice Sheet surface mass balance bias on uncertainty in sea level rise projections in 2100

APPROVED BY
SUPERVISING COMMITTEE:

Supervisor:

Donald D. Blankenship

Co-Supervisor:

Charles S. Jackson

Terrence M. Quinn

Luc L. Lavier

Effect of modeled pre-industrial Greenland Ice Sheet surface mass balance bias on uncertainty in sea level rise projections in 2100

by

Gail Ruth Gutowski, B.S.

Thesis

Presented to the Faculty of the Graduate School of

The University of Texas at Austin

in Partial Fulfillment

of the Requirements

for the Degree of

Master of Science in Geological Sciences

The University of Texas at Austin

August 2013

Dedication

This thesis is dedicated to Brian Muldoon, whose belief in me is endless. Thanks for seeing me through yet another milestone.

Acknowledgements

I would like to thank my research advisors, Charles Jackson and Don Blankenship for their continued support. This work would not have been possible without their feedback and encouragement and I look forward to working with them on my Ph.D. Thanks also to Terry Quinn and Luc Lavier for serving on my Master's Thesis Committee; I greatly appreciate their willingness to help me achieve my academic goals.

I also acknowledge my collaborators on the Community Ice Sheet Model for their input and feedback on topics related to this work: Bill Sacks for guidance in running the model and for tireless model development in response to the needs (and requests) of users such as myself; Jeremy Fyke and Miren Vizcaíno for useful conversations and work relating to model initialization and surface mass balance considerations; and Bill Lipscomb for being a mastermind behind CISM and providing valuable scientific insight;

My officemates for the past year (Marie Cavitte, Chad Greene, and Enrica Quartini) provided immeasurable moral support in the completion of this thesis. Thanks to Kaustubh Thirumulai for instigating this master's and also providing guidance along the way. Thanks to all of the scientists and staff at UTIG who make this an enjoyable and rich environment in which to do science. A special thank you to the UTIG "gripe" team, in particular Mark Weiderspahn, for his relentless IT support without which I would have had many more sleepless nights.

As with most things in life, science doesn't come free. Funding for this project was provided by NSF Cyber-enabled Discovery and Innovation Grant #0941678, the Fred M. Bullard Student Research Fund, and the UT Jackson School of Geosciences.

Finally, I would like to thank my family for their unwavering support over the years and for constant reminders over the last few months that I "better finish" my thesis.

Abstract

Effect of modeled pre-industrial Greenland Ice Sheet surface mass balance bias on uncertainty in sea level rise projections in 2100

Gail Ruth Gutowski, M. S. Geo. Sci.

The University of Texas at Austin, 2013

Supervisor: Donald Blankenship

Co-Supervisor: Charles Jackson

Changes to ice sheet surface mass balance (SMB) are going to play a significant role in future sea level rise (SLR), particularly for the Greenland ice sheet. The Coupled Model Intercomparison Project Phase 5 (CMIP5) found that Greenland ice sheet (GIS) response to changes in SMB is expected to contribute 9 ± 4 cm to sea level by 2100 (Fettweis et al 2013), though other estimates suggest the possibility of an even larger response.

Modern ice sheet geometry and surface velocities are common metrics for determining a model's predictability of future climate. However, care must be taken to robustly quantify prediction uncertainty because errors in boundary conditions such as SMB can be compensated by (and therefore practically inseparable from) errors in other aspects of the model, complicating calculations of total uncertainty.

We find that SMB calculated using the Community Earth System Model (CESM) differs from established standards due to errors in the CESM SMB boundary condition. During the long ice sheet initialization process, small SMB errors such as these have an opportunity to amplify into larger uncertainties in GIS sensitivity to climate change.

These uncertainties manifest themselves in ice sheet surface geometry changes, ice mass loss, and subsequent SLR.

While any bias in SMB is not desirable, it is not yet clear how sensitive SLR projections are to boundary condition forcing errors. We explore several levels of SMB forcing bias in order to analyze their influence on future SLR. We evaluate ensembles of ice sheets forced by 4 different levels of SMB forcing error, covering a range of errors similar to SMB biases between CESM and RACMO SMB.

We find that GIS SMB biases on the order of 1 m/yr result in 7.8 ± 3.4 cm SLR between 1850 and 2100, corresponding to 100% uncertainty at the 2σ level. However, we find unexpected feedbacks between SMB and surface geometry in the northern GIS. We propose that the use of elevation classes may be incorrectly altering the feedback mechanisms in that part of the ice sheet.

Table of Contents

1. Introduction

Sea level rise is observed to be accelerating in response to global climate change, putting people and economies at risk (Church et al. 2006, Nicholls et al. 2010). Planning for this risk demands careful accounting of uncertainty in sea level rise (SLR) projections. Estimates have placed a "reasonable" upper bound of 2 meters on 21st century SLR (Pfeffer et al. 2008). However, many sources of uncertainty have been omitted in this estimate, suggesting that the upper bound on future sea level rise is still unconstrained (Rahmstorf 2010). For example, a more thorough accounting of ocean processes and uncertainty have driven estimates higher, suggesting an upper bound on total SLR by 2100 of 2.25 m (Sriver et al. 2012). The contribution of ice sheet dynamics to SLR projections has largely been ignored until recently, but is expected to further increase estimates of the upper bound on SLR during the next century (e.g. Bindschadler et al. 2013).

In addition to ocean thermal expansion and ice dynamics, melting of land ice cover is a main contributor to rising sea level. Mountain glaciers are experiencing accelerated melt in response to modern (post-1850) climate change and many are predicted to disappear as early as 2050 (Paul et al. 2004). Ice sheets such as Greenland and Antarctica, which contain ice mass equivalent to approximately 64 meters of SLR (IPCC 2007), have slower response times and are more resilient to climate change than mountain glaciers due to their large size. However, accelerating mass loss is observed in Greenland and parts of Antarctica over timescales of a decade or shorter, making them potentially important suppliers of melt water that may raise sea level by an additional 50 cm or more over the next century (Rignot et al. 2011). Even higher rates of ice sheet contribution to sea level are possible, but scientific underpinnings for such arguments are more speculative at present.

The effect of changes in surface mass balance (SMB) is particularly important when considering Greenland ice mass loss. SMB accounts for net changes to the ice sheet surface, including precipitation and ablation effects. The calculation of SMB neglects basal influences, which are not well understood physically (e.g. Larour et al. 2012). Mass loss from the Greenland ice sheet (GIS) since pre-industrial times is caused primarily by increased surface melting and acceleration of outlet glaciers, as revealed by gravity measurements (van den Broeke et al. 2009). Unprecedented surface melting in Greenland has been recorded over the last few years, with melting observed over 95% of the GIS surface in summer 2012 (Hall et al. 2013). The Coupled Model Intercomparison Project Phase 5 (CMIP5) found that GIS SMB is expected to contribute ~ 9 ± 4 cm to sea level by 2100 (Fettweis et al 2013). Therefore, we expect accurate modeling of Greenland SMB to be important for constraining future SLR.

Though SMB is a critical element of understanding the future state of the GIS, it is also a source of uncertainty for future projections of ice sheet evolution and SLR. By nature, SMB observations of the future are unavailable. In the absence of future observations to use as forcing, imposing an SMB boundary condition in ice sheet models is a challenge. This is due to the complexity of accurately modeling all of the relevant physical processes such as surface evolution and feedbacks between the atmosphere and the ice sheet surface. In lieu of observations, climate models must be relied upon to calculate an SMB boundary condition that is self-consistent with the equilibrated model ice sheet, while reflecting appropriate ice physics. The quality of a model-derived SMB boundary condition is evaluated against past observations of SMB represented by regional models such as the Regional Atmospheric Climate Model (RACMO; Ettema et al. 2009). The resulting modeled SMB is inherently uncertain due to errors in both observations and model physics, which are expected to contribute to errors in ice sheet surface geometry and projected SLR.

There are many sources of uncertainty in predicting SLR. Modeling feedbacks at the ice-ocean interface is challenging and is often rudimentary or neglected entirely, though it is important for fully capturing the effects of ice dynamics on mass loss. However, previous work has shown that ice-ocean coupling is most important in Antarctica and has minimum impact in Greenland (see discussion in Lipscomb et al. 2013). Uncertain flow physics is another potential source of uncertainty; the material properties of ice are still not well understood under all conditions and unknown basal conditions contribute to uncertainties in ice dynamics. Flow physics is intentionally simplified in ice sheet models for computational reasons, to improve model efficiency and numerical stability.

SMB is not the only boundary condition required by ice sheet models; subglacial hydrology and basal topography are additional examples of uncertain boundary condition forcings. Due to the difficulty inherent in observing englacial and subglacial properties of the ice sheet, it is necessary for models to account for these basal conditions from indirect sources, introducing additional uncertainty into the system. Finally, ice sheet initial conditions are not well constrained. Approaches to ice sheet model initialization vary widely between model implementations. The selection of initial condition parameters, for example, relies on the choice of metrics used to evaluate optimal solutions of model parameters. The development of appropriate ice sheet model initialization procedures is an active area of research.

While there are many factors that may affect uncertainty in SLR estimates produced by our model (such as the lack of higher-order physical processes, uncertain boundary conditions, and initial parameter estimation), we focus on the SMB boundary condition because it is a primary driver of GIS ice mass loss. Anomalies between modeled and observed ice sheet geometry, elevation, and velocity suggest that any subsequent projected ice sheet will be uncertain, though it is not yet clear how pre-industrial SMB errors will manifest quantitatively in future projections. Lipscomb et al.

(2013) show that large biases exist in SMB calculated using the Community Earth System Model (CESM), though it is unclear how these may affect SLR predictions. Previous work has shown equilibrated geometry is sensitive to SMB biases (e.g. Pollard 2000, Fyke et al. 2011). While we assume that our initialized model is in steady state with its boundary conditions, the initialization process may provide enough time for initially small errors in SMB to become large errors in ice sheet geometry, leading to large uncertainty in SLR predictions.

If SLR uncertainty in year 2100 scales with pre-industrial SMB errors, reducing errors in pre-industrial SMB should reduce uncertainty in future SLR projections. By modeling ice sheet evolution from 1850 to 2100, we quantify uncertainty in future SLR based on a range of errors in the SMB boundary condition, which are representative of the types of SMB biases that exist between CESM climate and estimates of SMB from RACMO. We also calculate the sensitivity of surface projected geometry anomalies to pre-industrial SMB forcing anomalies to demonstrate the strength of the feedback between these processes.

2. Model Description

2.1 Community Earth System Model

The Community Earth System Model (CESM) is a general circulation model (GCM) incorporating individual climate components – atmosphere, ocean, land, sea ice, and land ice – to create a coupled climate model. CESM therefore benefits from using established standard models developed by experts in each research community.

The sub-models interact through a coupler designed to allow feedbacks between different components of the global system. Within CESM, there are two relevant modes of operation for each sub-model: data and active. A configuration employing a data sub-model is one in which the role of the model is replaced by appropriate data fields that were derived from observations or previously calculated by another iteration of CESM. An active sub-model is one in which the output fields are dynamically computed during runtime, as they would be in a stand-alone model.

2.2 Community Ice Sheet Model

The Community Ice Sheet Model (CISM; Lipscomb et al. 2013) is the ice sheet sub-model within CISM. It is an extension of the Glimmer ice sheet model (Rutt et al. 2009), further developed for coupling to CESM. CISM was selected to be the standard ice sheet model for CESM because of the generalizability of its construction, ongoing efforts to incorporate higher order physics, and the existence of a convenient coupling interface. It is the latest sub-model to be incorporated into the CESM framework, but its inclusion has been under development at the Los Alamos National Laboratory and the National Center for Atmospheric Research since 2009.

CISM 1.0 uses the shallow ice approximation (SIA) to the Navier-Stokes equations under the limit of small Reynolds number. In this limit, inertial (momentum) forces are negligible compared to viscous forces. The equations of ice flow solved by the model are conservation of mass, linear momentum, and internal energy (Rutt et al. 2009):

$$\nabla \bullet u = 0 \quad (1)$$

$$\rho \frac{d\mathbf{u}}{dt} = \nabla \bullet \sigma + \rho g \quad (2)$$

$$\rho \frac{d(c_p T)}{dt} = \nabla(k \nabla T) + \boldsymbol{\phi} \quad (3)$$

Here ϱ is ice density, u is three-dimensional ice velocity, T is temperature in degrees Celsius, g is gravitational acceleration, σ is the stress tensor, c_p is the specific heat of ice, k is thermal conductivity of ice, and $\boldsymbol{\phi}$ is the deformational heat in ice. Glacial ice in CISM is assumed to be a fluid that is incompressible, heat-conducting, viscous, and non-Newtonion. SIA accounts for vertical shear, but neglects lateral and longitudinal stresses that may be important in regions of fast ice flow. While higher-order terms in the governing equations including all englacial stresses would be ideal, the SIA is reasonable for the GIS, which does not include ice shelves, unlike the Antarctic Ice Sheet (AIS). CISM 1.0 has not been applied to the AIS in part because of the SIA limitation, which is considered insufficient for capturing the more complex feedbacks from ice shelves and ice—ocean interactions.

Ice sheet surface boundary conditions in CESM, such as temperature and SMB, are calculated by the Community Land Model (CLM; Oleson et al. 2010) with input from the Community Atmosphere Model (CAM; Neale et al. 2011), downscaled, and passed to CISM via one-way coupling. CISM is unique in its energy-balance SMB calculation, discussed in Section 2.1. Other ice sheet models employ the positive-degree-day (PDD) scheme to approximate SMB (Braithwaite 1995). The energy-balance method assumes that the empirically derived relationship between melting and the sum of degrees above freezing in a day is both linear and unchanging through time. This assumption is not likely to hold for a changing climate. It may instead seem better to predict SMB through

consideration of the factors contributing to melt, however it could be that additional errors could be introduced if a climate model is not predicting those factors correctly.

The Paterson-Budd formulation of the Glen-Nye constitutive relationship (Paterson and Budd, 1982), used to determine components of the stress tensor is given by

$$\varepsilon'_{ij} = A(T)\,\tau_e^{n-1}\,\tau_{ij} \qquad (4)$$

where ε'_{ij} is the strain rate tensor, A is the empirically-derived, temperature-dependent rate factor (Payne et al. 2000), τ_e is the effective stress, and τ_{ij} is the stress deviator tensor. The Glen law exponent is typically chosen to be $n = 3$ for glacial ice, based on empirical data.

Table 1 shows the CISM configuration parameters used in this study. Geothermal flux, basal sliding, and "flow enhancement factor" constants are calculated using a simple optimization procedure in which parameters are ranked by how well they minimize model-data discrepancies in GIS volume and extent (Lipscomb et al. 2013). We apply constant geothermal flux of $G = 0.062$ W/m2 over the entire ice sheet and a flow enhancement factor of $f = 2.75$ (Lipscomb et al. 2013). For numerical stability, ice dynamics are evaluated only where the ice sheet is at least 100 m thick.

Initial basal topography and ice thickness are taken from Bamber et al. (2001), with additional high-resolution data in the region of Jakobshavn Isbrae (CReSIS 2010). In our configuration, basal hydrology is neglected and basal sliding is controlled by a constant basal sliding parameter. When basal ice reaches the pressure melting point, ice velocity is assumed to be linearly proportional to driving stress in the ice. Below the pressure melting point, sliding is not permitted. The optimized basal sliding parameter we use is B = 3.42 yr-1 Pa-1.

Mass loss through calving in the model is equivalent to runoff of solid ice. A simple calving parameterization is used so that ice thickness goes to zero when ice goes

afloat as defined by Archimedes' principle. The model therefore cannot include ice shelves, which are not observed on the GIS.

Full coupling between CISM and other CESM model components is still under development. One-way coupling exists between CISM and CAM. This is sufficient for our study because we apply a data atmosphere to force our calculation of SMB, which does not allow for active feedback between the ice sheet and atmosphere.

2.3 Surface Mass Balance Calculation

Instead of a PDD approach, CISM uses an energy balance scheme to calculate SMB in a changing climate. SMB is calculated in CLM for 10 elevation classes per land grid cell. Elevation classes divide grid cells over the ice sheet at set elevations, with lower bounds at 0, 200, 400, 700, 1000, 1300, 1600, 2000, 2500, 3000, and 10000 meters. These classes allow for the resolution of ice sheet surface slopes that are otherwise too steep for the 1° (~110 km) CLM grid to capture. Daily SMB results are accumulated and averaged over each grid cell for 1 year before being downscaled from the CLM grid to a finer 5 km ice sheet grid. Lipscomb et al. (2013) discuss the downscaling process in more detail. CISM uses SMB calculated by CLM as a surface boundary forcing when updating ice sheet area and extent for each model year. Evaluating SMB over the coarser CLM grid and then downscaling is less computationally expensive than evaluating over the finer CISM mesh by a factor of at least ten (Lipscomb and Sacks, 2012). This approach also allows for the use of CLM's sophisticated snow physics parameterization.

The calculation of snow and ice SMB is discussed in detail in Vizcaíno et al (2013). The SMB passed to CISM is that of ice only and does not include the SMB of snow other than to record the conversion of snow to ice. Future versions of CISM are expected to handle SMB from both snow and ice, as per the common definition. A special glacier class has been incorporated into the standard CLM SMB scheme to improve estimates of ice SMB (Lipscomb et al. 2013). For example, a maximum snow

depth is enforced in the standard CLM such that snow in excess of 1 meter liquid water equivalent (LWE) depth instantaneously runs off to the ocean. However, in the case of glacial ice, snow in excess of the 1 m LWE threshold is instead converted to ice which adds positive SMB. In effect, this takes the place of a snow firn model, which CLM lacks. In the standard CLM, meltwater remains in place where it may refreeze depending on ice sheet temperature conditions. In the case of glacial ice, on the other hand, meltwater from ice runs off instantaneously to the ocean, which leads to a negative contribution to SMB.

The calculation of ice SMB is therefore taken to be:

$$SMB(ice) = SC - ME \tag{5}$$

where SC is the representation of snow compaction in the absence of a firn model (see above) and ME is melting. Surface melting is derived from the balance of surface fluxes:

$$ME = SW_d(1 - \alpha) + LW_d - \varepsilon \sigma T_s^4 + SHF + LHF + GF \tag{6}$$

where SW_d is downwelling shortwave radiation, α is albedo, ε is the emissivity of the ice sheet surface, σ is the Stefan-Boltzman constant, T_s is surface temperature, LW_d is downwelling longwave radiation, *SHF* is sensible heat flux, *LHF* is latent heat flux, and *GF* is the upward geothermal flux.

Coupling between CLM and CISM is currently one-way, such that surface topography is not updated in response to changes in ice dynamics in CISM. However, the model does include limited elevation feedbacks through the effect of an assumed atmospheric lapse rate. A lowered ice sheet surface would estimate a new SMB based on a higher air temperature given the elevation class parameterization used for estimating SMB at sub-CLM-grid scales. This limitation is permissible for evolution over short

timescales (less than 100 years), but may have an effect on longer runs with larger elevation changes. To accommodate this, two-way coupling between CISM and CLM is under development.

3. Methods

3.1 Surface Mass Balance Forcing

We calculate SMB using CESM to obtain appropriate forcing for our ice sheet spinup and 1850 - 2100 runs. This provides consistent future SMB forcing in equilibrium with our initialized ice sheet. The model is configured so that CLM and CISM components are forced by a pre-industrial data atmosphere, known internally to CESM as the "IG1850" component set. The atmosphere forcing is 3-hourly output from the Mother of All Runs (MOAR) dataset, the result of a previous run of CESM with coupling between atmosphere, ocean, land, and sea-ice components and boundary conditions appropriate to 1850.

We use 155 years of pre-industrial atmospheric MOAR output repeated once to force our calculation of the pre-industrial SMB field for the GIS. The data is looped to provide a longer forcing period in an effort to mitigate the effect of transients and establish equilibrium snow depths. The result is the 310-year "perpetual" pre-industrial SMB timeseries shown in Figure 1. Figure 2 shows the average CESM SMB field. As Vizcaíno et al. (2013) discuss, our calculated SMB compares favorably to observations, though biases exist between RACMO and CESM along the margins. Additional biases in ice growth are observed along the northern margin (Lipscomb et al. 2013). Because the ice masks differ between CESM and RACMO, we compute the anomaly between the two models only where the ice masks are coincident. Therefore, the bias in ice extent outside the RACMO ice mask is not shown in Figure 2. The SMB calculated by CLM was downscaled and passed to CISM once per model year. The calculation assumes an observed present-day GIS geometry based on Bamber et al. (2011). Ice sheet dynamics were turned off during this integration to separate the calculation of SMB from the execution of CISM.

From the last year in the perpetual pre-industrial SMB timeseries, we continued the integration from 1850 to 2005, using the comparable "IG20c" component set in CESM. This run was forced by atmospheric MOAR forcing output from a previous run based on observed forcing from the same time period. Finally, CLM was integrated from 2005 to 2100 using available CESM atmospheric output that reflects (Representative Concentration Pathways (RCP) 8.5 emissions forcing. RCP 8.5 corresponds to a radiative forcing of 8.5 W/m^2. It most closely relates to the A2 emissions scenario, one of the higher emissions trends evaluated for the 2007 report of the Intergovernmental Panel on Climate Change (IPCC 2007).

With some important limitations, the resulting pre-industrial SMB could provide a valuable SMB forcing to users of other ice sheet models.

3.2 Surface Mass Balance Forcing Bias

We find a bias in CESM pre-industrial SMB as compared to a community standard, the Regional Atmospheric Climate Model (RACMO; Ettema et al. 2009). RACMO is a regional atmospheric GCM forced at its boundaries by reanalysis data produced by the European Centre for Medium-Range Weather Forecasts (ECMWF). Though a model product, RACMO SMB is akin to observations because it is thought to accurately represent SMB processes on a relatively high-resolution grid (11 km) in the region of the GIS. We use it here as a convenient metric for defining an 1850 SMB bias characteristic of CESM.

Figure 3 shows the SMB anomaly between CESM and RACMO. Anomalies are close to zero in the interior of the ice sheet, where ice is flowing slowly and accumulation dominates. Along the coasts, where SMB is nonzero and ablation zones are active, the average SMB anomaly discrepancy to RACMO is on the order of 1 meter. We consider the model-data discrepancy in SMB shown in Figure 3 to be representative of SMB boundary condition bias.

We expect our modeled pre-industrial SMB to be anomalous compared to any observed metric because CESM climate differs from observed. To examine the influence of a range of pre-industrial SMB biases on SLR projections from our model, we take advantage of the internal variability in our 310-year SMB perpetual 1850 timeseries. To quantitatively simulate biases, we deconstruct our 310-year SMB forcing dataset into 1-, 4-, 9-, and 16-year interval ensembles. For example, in 100 years of SMB data there are 97 possible samples of consecutive 4-year estimates of SMB. Any one sample can have significant error with respect to a long-term mean. Here we assume this error is persistent in time to simulate the influence of CESM-like SMB bias compared to the RACMO estimate in our model evaluation.

The standard deviation for each of these ensembles is shown in Figure 4. These SMB forcing periods were chosen because we expect noise in the signal to fall as $\frac{1}{\sqrt{N}}$. For example, we expect that the 4-year forcing period will have half as much noise as the 1-year forcing period. This effect corresponds to a reduced variance in longer forcing periods compared to shorter periods, as seen in Figure 4.

Coastal SMB anomalies seen in the 1-, 4-, 9-, and 16-year ensembles are 1.6 m, 1 m, 0.5 m, and 0.36 m, respectively. Therefore, the 4-year ensemble most closely corresponds to the CISM-RACMO SMB discrepancy shown in Figure 3. For this reason, we emphasize the 4-year ensemble in our analysis.

3.3 Experiment Design

To simulate the influence of bias in the pre-industrial SMB boundary condition on projections of SLR, we "introduce" known biases into our CISM runs via our choice of SMB forcing sample from the various SMB ensembles during the ice sheet initialization. Simulating biases characteristic of our model-data anomaly (Figure 3) is a simplification of the problem that allows us to explore the sensitivity of the model to a range of biases in the pre-industrial SMB boundary condition. We then examine how these biases are

reflected in the evolution of GIS surface geometry and how the resulting surface anomalies affect uncertainty the in CESM prediction of the GIS contribution to SLR.

Each of the 200 experiments (50 ensemble members in 4 ensembles) was initialized for 9900 model years using its respective SMB forcing. This run length (shorter than 10,000 years) was chosen for convenience given the CESM four-digit year output file naming convention, while allowing as much time as possible for the model to reach steady state. We acknowledge that ensuring equilibration during model spinup is an important consideration for appropriate model initialization. The ice sheet was initialized using the "TG1850" component set of the CESM model, which includes an evolving ice sheet with one-way coupling from CLM to CISM. It differs from the "IG" component set used to calculate SMB (see Section 3.1) in that there is no recalculation of SMB as that information is already incorporated in the SMB forcing and elevation classes. Additionally, our configuration of the TG run allows the ice sheet surface to evolve, whereas our estimate of SMB from the IG runs included no surface evolution feedback. Our ice sheet spinup and subsequent projection runs use a time step of 0.05 years.

Model integration was continued from the end of the spinup (year 1850) through 2100, using SMB from our IG run and including the influences of anthropogenic forcing from RCP 8.5 emissions conditions between 2005 and 2100. Together, the runs represent 200 model integrations of initialized GIS evolution between 1850 and 2100. For this time period, we analyze the SMB and ice sheet volume to derive GIS contribution to sea level change during the 21st century. Volume is calculated based on the integration of modeled ice thickness in each 25 km^2 grid cell. GIS volume loss is taken to be the volume difference in the modeled ice sheet compared to 1850. The ice volume loss is translated to a liquid water volume loss equivalent, assuming density of ice is $\varrho_i = 0.9167$ g/cm^3 and density of pure liquid water is $\varrho_w = 0.9998$ g/cm^3. We scale this value by the area of the world's oceans, $A_{ocn} = 3.6 \times 10^8$ km^2, to arrive at a SLR estimate, implicitly assuming equal spatial distribution of meltwater over the world's oceans.

4. Results

4.1 2100 Sea Level Rise and Uncertainty

Each of the 200 experiments in this study was initialized with its own SMB forcing, as discussed in Section 3.1. Figure 6 shows the resulting spunup pre-industrial GIS volume for each experiment, which were used as the initial state for each of 200 integrations of the ice sheet from 1850 to 2100. The SMB forcing after 1850 was the same for all experiments; however, variations in the initialized ice sheet geometry result in differences in the SMB applied to each ice sheet due to the dependence of SMB on elevation. The timeseries of net mean ice sheet SMB for each ensemble is shown in Figure 7.

Between 1850 and 2100, SMB becomes increasingly negative along most of the GIS coast, while SMB increases slightly in the interior of the ice sheet, as shown in Figure 8a. Areas of increased SMB roughly correspond to areas of slow ice flow (Figure 8c). With a warming atmosphere, we expect more precipitation. This has the potential to add mass to the ice sheet if temperatures are below freezing, a case more likely at higher elevation. Areas of negative SMB generally correspond to lower ice sheet surface elevation (Figure 8b). This is because air temperatures are warmer at lower elevations, which leads SMB to be more negative.

After 2050, the GIS SMB becomes more variable and generally negative. In all cases, the modeled ice sheet loses volume on the order of 3 x 10^4 km^3 (3 x 104 Gt) between 1850 and 2100. Of the 200 integrations, only 2 instances (both in the 1-year ensemble) produce an ice sheet that gains mass, and even those integrations begin losing volume rapidly after 2050, as demonstrated in Figure 9. The resulting mean SLR estimates in 2100 (Figure 10) are consistent within uncertainty between ensembles, with estimates ranging from 7.8 ± 3.4 cm (4-year ensemble) to 9.4 ± 5.1 cm (1-year ensemble). Table 2 summarizes the SLR projections and their associated uncertainty from

SMB initialization bias for each ensemble. As evident from Table 2, approximately 75% of the SLR occurs after 2005, consistent with an acceleration of mass loss and SLR over the next century. All ensembles exhibit 14% expansion in ablation area between 1850 and 2100, supporting the Lipscomb et al. (2013) result that increased ablation is a primary driver of mass loss during this time (Figure 11). This increase in ablation is in spite of the expectation that CESM will underestimate ablation due to the lack of some two-way feedbacks between the atmosphere and ice sheet models (Pritchard et al. 2008).

The 1σ standard deviation in 2100 SLR is shown in Figure 12. The uncertainty decreases with increasing forcing timescale, as expected from a reduction in noise in the SMB forcing. The 1-year forcing ensemble demonstrates the most variability in SLR indicating a GIS contribution to SLR of as much as 20 cm by 2100. Our mean SLR projections agree favorably with the result of the Control 3 experiment of the SeaRISE multimodel effort (Bindschadler et al. 2013), which most closely matches the RCP 8.5 emissions forcing used here. However, our uncertainty due to the ice sheet's sensitivity to changes in SMB is significant. At the ± 2σ level, indicative of the spread in 2100 SLR at 95% significance, even the lowest-SLR scenario (16-year forcing ensemble) exhibits uncertainty that is nearly 90% of the mean. In the most variable case (1-year forcing ensemble), uncertainty in 2100 SLR exceeds 200% of the mean value. This result indicates that errors in SMB at the time of ice sheet initialization are amplified significantly into SLR uncertainty in year 2100.

4.2 CESM Ice Sheet Feedbacks Between SMB and Surface Elevation

The relationship between SMB bias and the loss of mass from the GIS is complicated by a non-linearity between SMB and elevation change. If the relationship between SMB forcing and elevation response were linear, then SMB biases would not affect the results of any forcing experiment as the effects of bias would affect the end and initial states equally. However, SMB is strongly affected by elevation such that a loss of

ice volume will lower the surface elevation of the ice sheet and SMB could become more negative assuming temperatures warm. A positive SMB anomaly could likewise increase the elevation of an ice sheet and the fraction of precipitation that is snow. Both are examples of positive feedbacks. These two examples are reasonable expectations for what we could find in the CESM experiments, although, as it turns out, this is not the case for much of the ice sheet.

To analyze feedbacks between SMB bias and the GIS contribution to SLR between 1850 and 2100, we calculate anomalies in SMB and surface elevation changes from the ensemble mean of SMB forcing at the beginning and end of the ice sheet spinup and between 1850 and 2100: The ratio between the elevation change and SMB bias and elevation change gives a measure of the feedbacks. A value close to zero would indicate elevation change is independent of bias and the sign of the value indicates the sign of the feedbacks. The quantities of interest are

$$SMB_f(t_{start})' = SMB_i(\overline{t_{start}}) - \overline{SMB(t_{start})} \quad (7)$$

$$SMB_f(t_{end})' = SMB_i(\overline{t_{end}}) - \overline{SMB(t_{end})} \quad (8)$$

$$srf(t_{start})' = srf_i(\overline{t_{start}}) - \overline{srf(t_{start})} \quad (9)$$

$$srf(t_{end})' = srf_i(\overline{t_{end}}) - \overline{srf(t_{end})} \quad (10)$$

SMB_f' is the forcing SMB anomaly, where $\overline{t_{start}}$ indicates an average SMB over the first 400 years of the initialization period and $\overline{t_{end}}$ indicates an average SMB over the last 400 years of the initialization period. We use a 400-year average to reduce the influence of variability in our anomalies. Subscript *i* indicates a particular ensemble member, an apostrophe indicates an anomaly, and *srf* is the surface elevation of the ice

sheet. For simplicity, we limit the following analysis to anomalies for members of the 4-year ensemble only, which includes SMB forcing biases most similar to CESM-RACMO biases.

The southern part of the GIS shows expected feedbacks between SMB forcing at the beginning of the spinup and resulting surface elevation anomalies at the end of the spinup. An example of this is shown in Figure 13 for 20th member of the 4-year ensemble, though all ensembles we looked at show similar behavior. In the southern part of the ice sheet at the start of the spinup, there are positive SMB anomalies along the southeastern margin and negative SMB anomalies on the southwestern coast. These anomalies lead to corresponding positive and negative anomalies, respectively, in surface elevation at the end of the spinup. This behavior is expected because we expect that excessive SMB in a region will result in a higher elevation ice sheet.

The feedbacks for the northern half of the ice sheet, however, exhibit unexpected and inconsistent relationships between SMB forcing and elevation change. We present two cases in which individual ensemble members demonstrate opposite (negative) feedbacks locally in Northern Greenland.

The first example was taken from ensemble member 20 (out of 48 total members). The region in question (shown in Figure 14) is at the Northern margin of the GIS, an area coincident with anomalous in-situ ice growth. We focus on the feedbacks in SMB and surface elevation anomaly between the beginning and end of the 9900-year initialization period to analyze how biases in the ice sheet SMB forcing may be amplified during the spinup. Valleys in this region demonstrate anomalously high SMB during the first 400 years of spinup, which consumes much of the area by the last 400 years of spinup. Positive SMB anomalies lead to anomalously high surface elevation, as expected. The raw SMB over the valleys is positive, as is the ensemble mean, making the interpretation of the SMB anomaly straightforward: for this ensemble member, there is more SMB at lower elevations than average in this region of the Northern coast of the GIS. This is

counterintuitive to the anticipated feedback; we expect that low points on the ice sheet, such as valleys, would reflect a low SMB anomaly due to the dependence of SMB on elevation. At higher elevations, colder air temperature is expected to contribute to higher ice SMB, while at lower elevations, warmer air temperature would correspond to lower ice SMB.

A second example shows an alternate ensemble member (30; Figure 15) that exhibits what occurs when the same area is dominated by a positive SMB anomaly. This ensemble member also demonstrates an unexpected relationship between SMB forcing and surface elevation at the beginning and end of the spinup. In this ensemble member, the SMB anomaly pattern changes dramatically between the beginning and end of the spinup period. On average, during the first 400 years of spinup, the SMB and elevation anomalies are similar, both positive in the southern and southeastern part of the region of interest. However, averaged over the last 400 years of the spinup, the two no longer appear correlated, contrary to expectations. At the end of the initialization period, nearly the entire area exhibits anomalously low surface elevation compared to the ensemble mean, despite the fact that the positive SMB anomaly becomes more pronounced. This is the opposite of what we would expect, showing SMB anomalies driving surface elevation up in the lower elevations and down in the upper elevations.

4.3 Sensitivity of Ice Sheet Mass Changes to SMB Forcing Bias

Though an exhaustive search has not been completed to identify all such instances of the two examples described above, our results show that in general, the southern half of the GIS displays the expected positive feedback behavior, while feedbacks in the northern part of the ice sheet are less easily interpreted.

To explore this effect further and extend its impact to projections, we calculate the sensitivity of the anomalous change in surface elevation between 1850 and 2100:

$$\Delta srf' = [srf_i(t = 2100) - srf_i(t = 1850) - [\overline{srf(t = 2100) - srf(t = 1850)}] \quad (11)$$

to SMB at the beginning of the initialization period (equation 7). In equation 11, t = 1850 and t = 2100 correspond to those years in the model projection run. A collection of randomly-selected points around the GIS were used to confirm linear sensitivity between 1850 SMB forcing and 2100 surface elevation across ensemble members. At each point on the 5 km ice sheet grid, we estimate sensitivity to be the slope of the least-squares best fit line between 1850 SMB anomalies and 2100 surface elevation anomalies for all ensemble members, as demonstrated for an example point in Figure 5. All anomalies in this analysis are discrepancies between individual members of the 4-year ensemble and the corresponding ensemble mean.

The resulting sensitivity map is shown in Figure 16. We hypothesize that positive SMB anomalies during initialization would lead to anomalously large changes in surface elevation and vice versa. For example, excessive SMB during initialization would lead to anomalously high elevation by 2100 and anomalously low SMB forcing would contribute to anomalously low elevation by 2100. Both of these scenarios correspond to a positive sensitivity. As Figure 16 shows, however, we see a large region of negative sensitivity in the northern half of the GIS.

We have not found a physical explanation for this counterintuitive result. One alternative explanation may be that the application of elevation classes in the model introduces erroneous feedbacks. As discussed in Section 2.3, the CESM ice sheet includes the calculation of SMB in different elevation classes to enable a more realistic calculation and downscaling of SMB between the coarser CLM/Community Atmosphere Model grid and the finer ice sheet grid. It is possible that the implementation of the elevation classes or the downscaling itself leads to incorrect behavior at higher latitudes where assumptions of the chosen lapse rate may differ from what is occurring in CESM.

We confirm there is an unexpected vertical gradient in SMB between 700 and 3000 meters elevation, corresponding to elevation classes 4 and 8 (out of 10). The resulting distribution, shown in Figure 17, reveals an obvious distinction between vertical gradients in the northern and southern parts of the ice sheet.

5. Conclusions

Under RCP 8.5 conditions, CESM predicts eustatic sea level to rise 8.7 ± 5.1 cm between 1850 and 2100, according to the 200 experiments we conducted. All of our ensemble-mean estimates of SLR by 2100 agree to within uncertainty. We find evidence that the size of SMB errors introduced during ice sheet initialization have an effect on uncertainty in 2100 SLR projections. Namely, larger SMB forcing errors correspond to larger uncertainty in 2100 SLR, as shown in Figure 12.

The physical mechanism for this response in the lower latitude portions of the ice sheet fit the notion that negative SMB biases result in greater mass loss because of an acceleration in melt that occurs in lower elevations. However, we see multiple examples of regions in Northern Greenland that exhibit counterintuitive feedbacks between SMB forcing bias and surface elevation anomalies at the beginning and end of the initialization period. One proposed explanation for this is that model structure related to the use of elevation classes may have an unintended latitudinal effect, perhaps on differences in assumed lapse rate, on the ice sheet sensitivity to SMB forcing. This problem may partly explain why CESM is biased toward excessive ice growth along the Northern GIS margin.

We present results from the first CESM ensemble projections of 21st century SLR. Performing ensemble analysis in this way provides a tool for quantifying intramodel uncertainty and climate sensitivity. Our experiment design includes a novel statistical approach to simulating SMB forcing errors in an effort to explore the effect those errors have on estimates of SLR. However, we were unable to determine a consistent picture of how SMB forcing biases affect 21st century ice sheet surface elevation changes. In turn, we are unable to determine the mechanism through which SMB forcing errors will influence 2100 SLR estimates. However, our results reveal that

SMB forcing biases do get amplified during model initialization and impact projections of SLR by 2100.

Errors in the SMB forcing, as with any boundary condition, are unavoidable. To perfectly replicate observations, both our model and the observations themselves would need to be perfect, which is an impractical assumption. In the case of a complex physical system such as an ice sheet, it is possible for a range of model configurations forced by different boundary conditions to resemble observations. Given the observational standard as a measure of model success, all solutions in this range are equally valid. The distribution of valid solutions is expected to include the true boundary conditions, but without observations it is not possible to identify which configuration is most realistic, in the presence of unquantified uncertainties. The ambiguity of getting the "right" model configuration (which results in an ice sheet that matches observations) for the "wrong" reasons (such as unrealistic boundary conditions) can be attributed in part to both uncertainty in the boundary forcing and compensating errors.

Figures

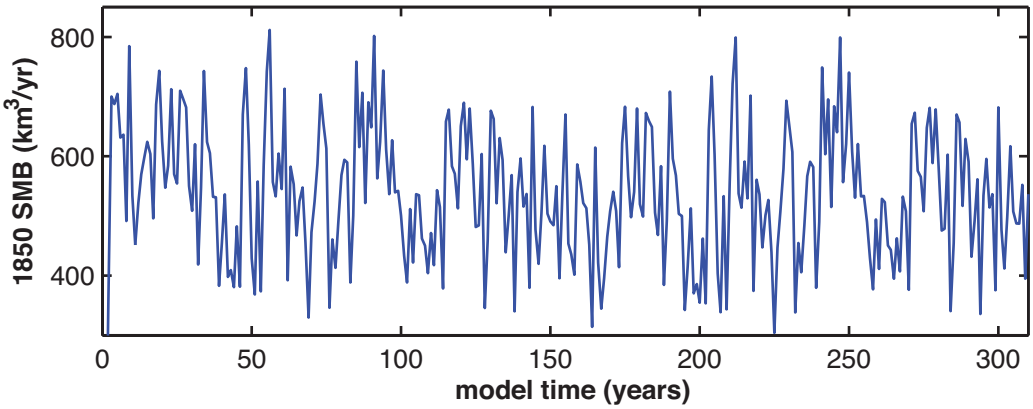

Figure 1: Annualized GIS surface mass balance calculated by CLM using pre-industrial forcing. 155 years of MOAR atmospheric forcing was repeated to force the SMB calculation. Samples of this SMB were used to force 200 ice sheet integration experiments described in this study.

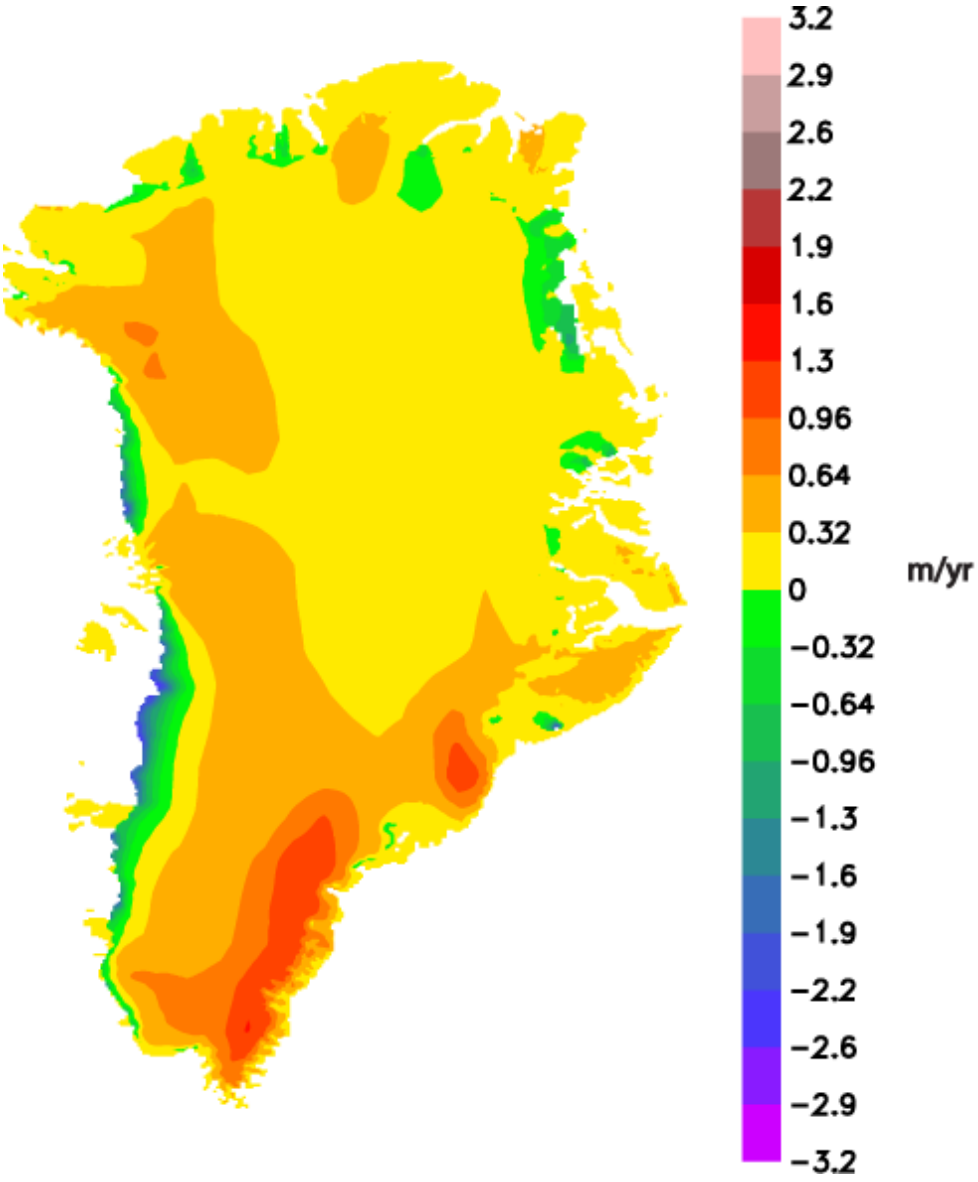

Figure 2: Mean pre-industrial (1850) Greenland surface mass balance generated using the Community Earth System Model. More extreme values of surface mass balance are found near coastal ablation zones, as expected. The lack of nonzero SMB at the northern margin is likely due to an imperfect ice mask. We show our data using the same ice mask used for RACMO to allow for comparison between the two.

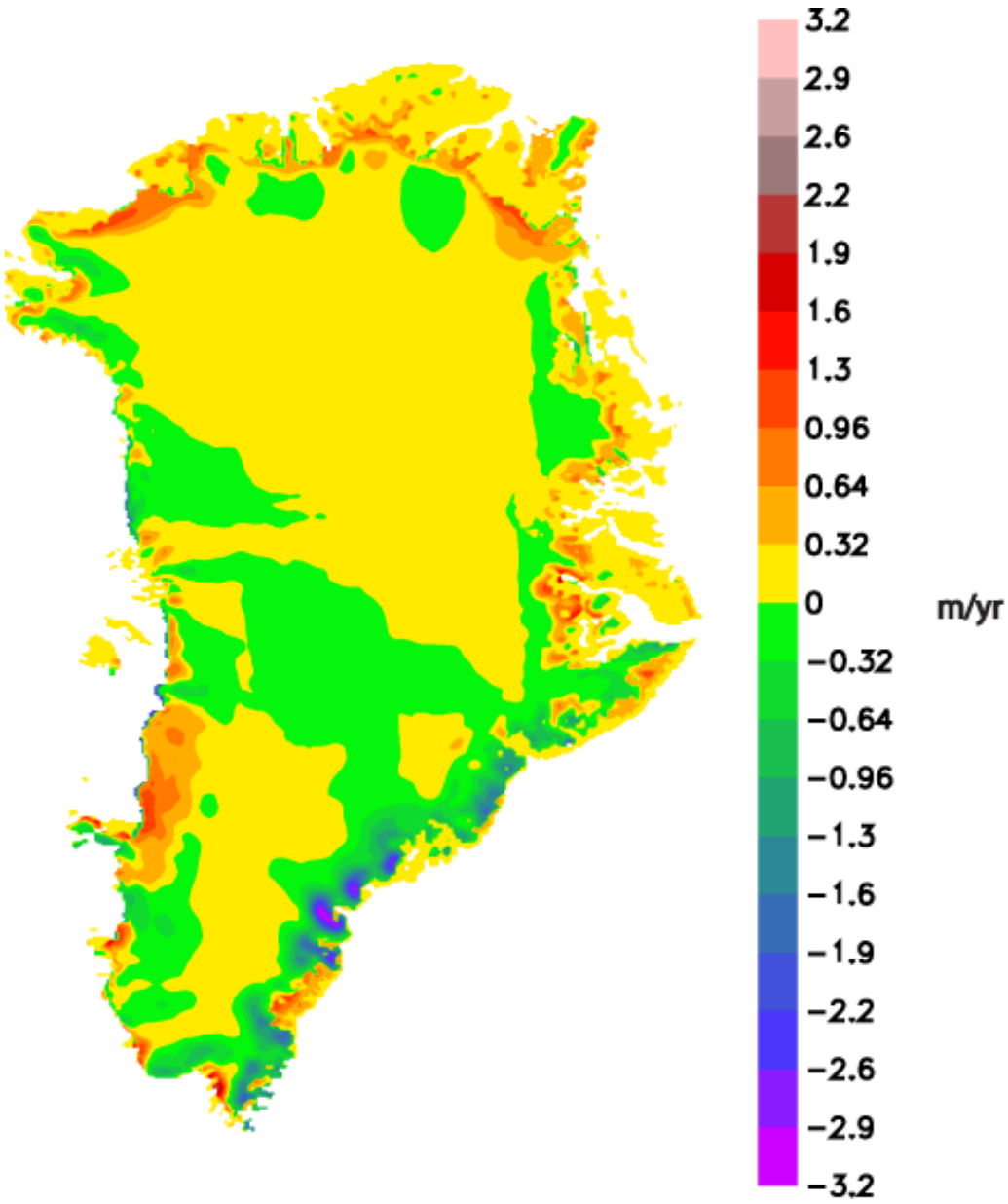

Figure 3: Anomaly between CESM and RACMO pre-industrial surface mass balance, calculated as CESM SMB minus RACMO SMB. CESM generally represents GIS SMB well compared to RACMO. In the coastal regions, anomalies are on the order of ± 1 meter.

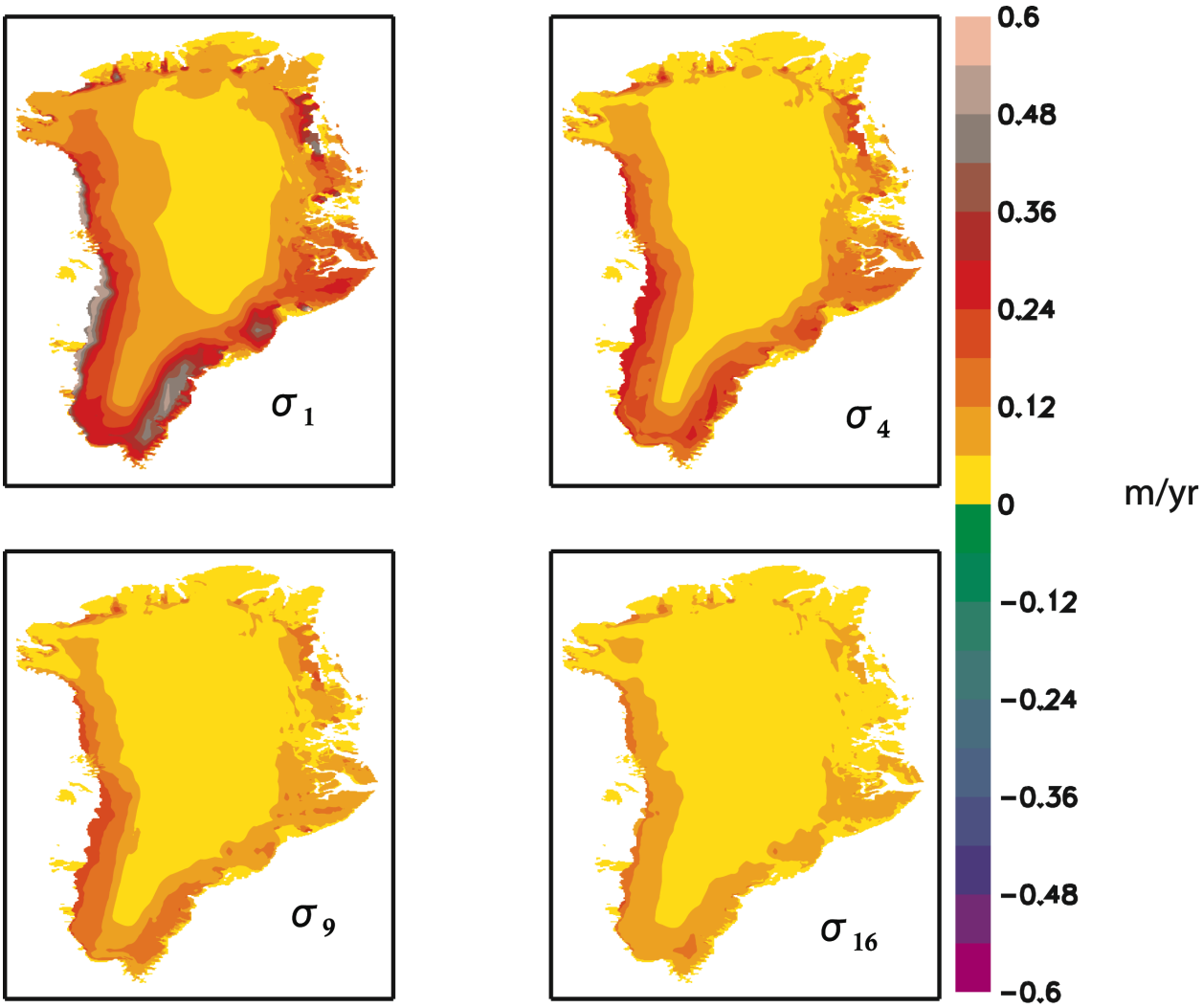

Figure 4: 1σ standard deviation of pre-industrial surface mass balance averaged over 4 timescales: 1 year (upper left), 4 years (upper right), 9 years (lower left), and 16 years (lower right). Note that at the 2σ level the 1- and 4- year timescales are well matched to the CISM-RACMO anomaly shown in Figure 2.

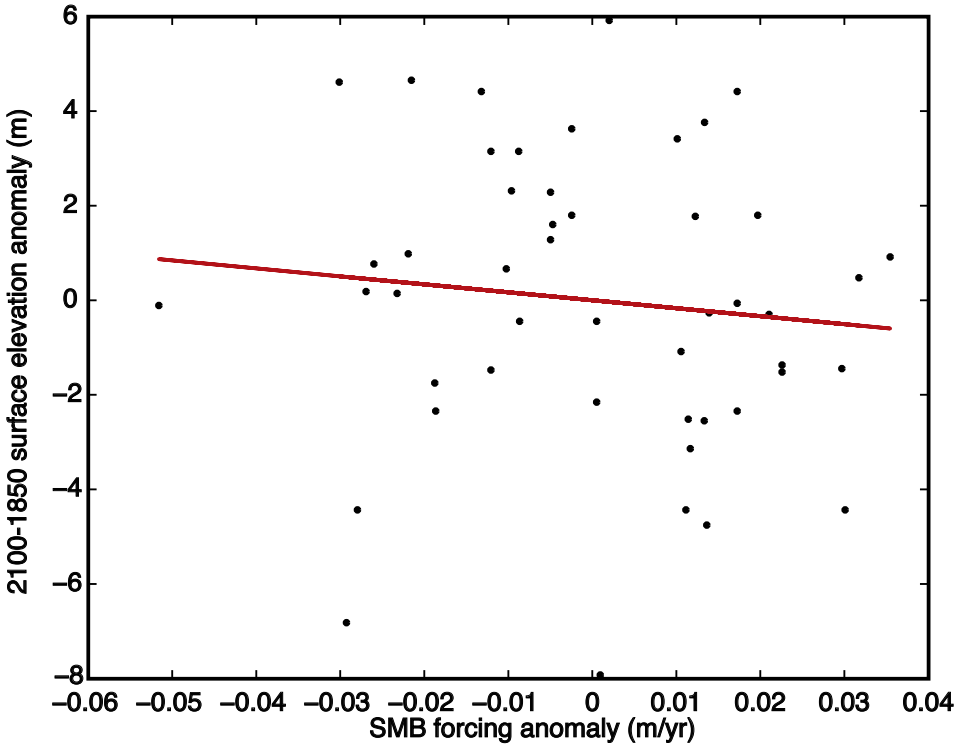

Figure 5: Example of the sensitivity fit for one grid point. The sensitivity is taken to be the slope of the least-squares best fit line which relates the anomaly in surface elevation change between 1850 and 2100 and the SMB forcing anomaly averaged over the first 400 years of the initialization period.

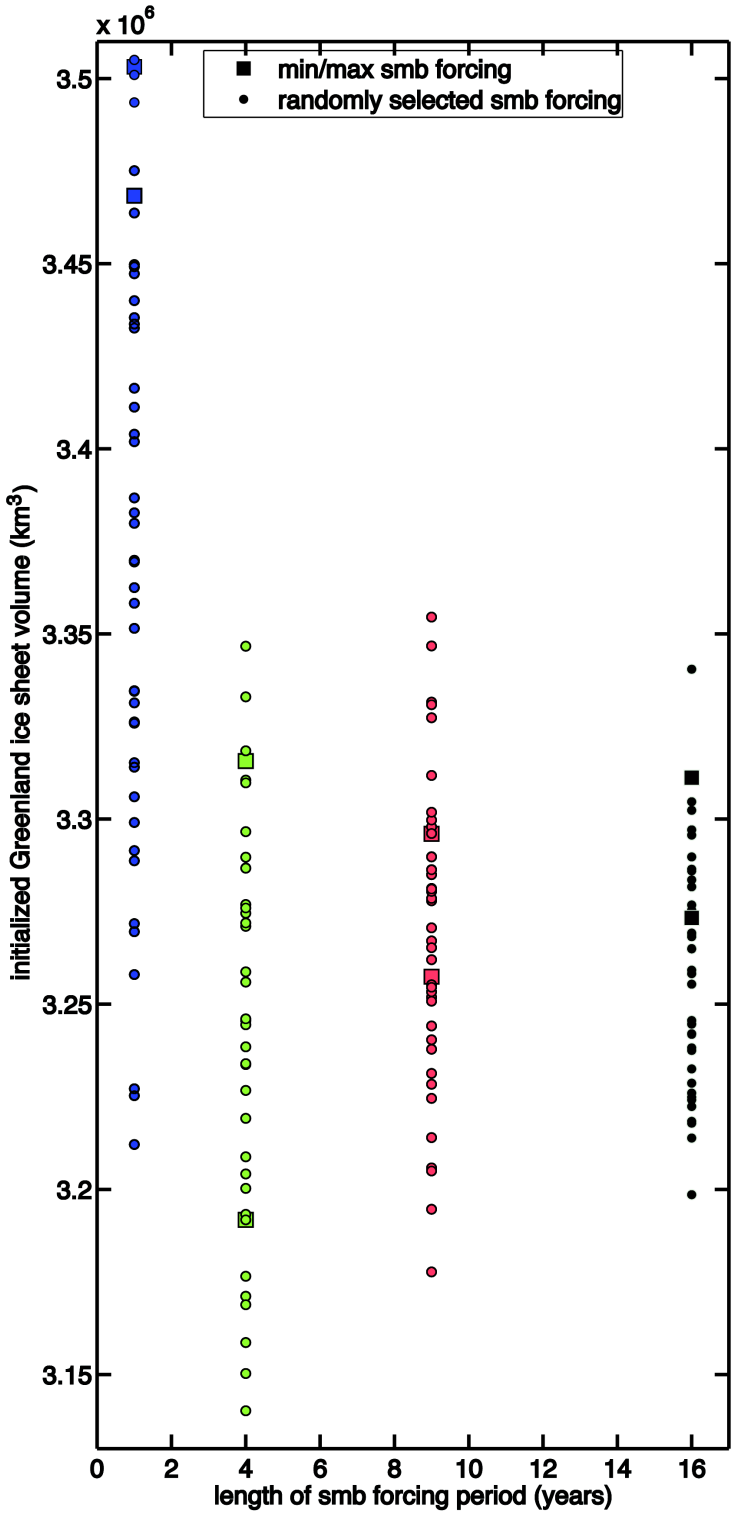

Figure 6: 1850 surface mass balance for each experiment at the end of the initialization period. Squares indicate runs that were initialized with a minimum or maximum surface mass balance for a particular ensemble. Circles indicate a randomly sampled initial surface mass balance.

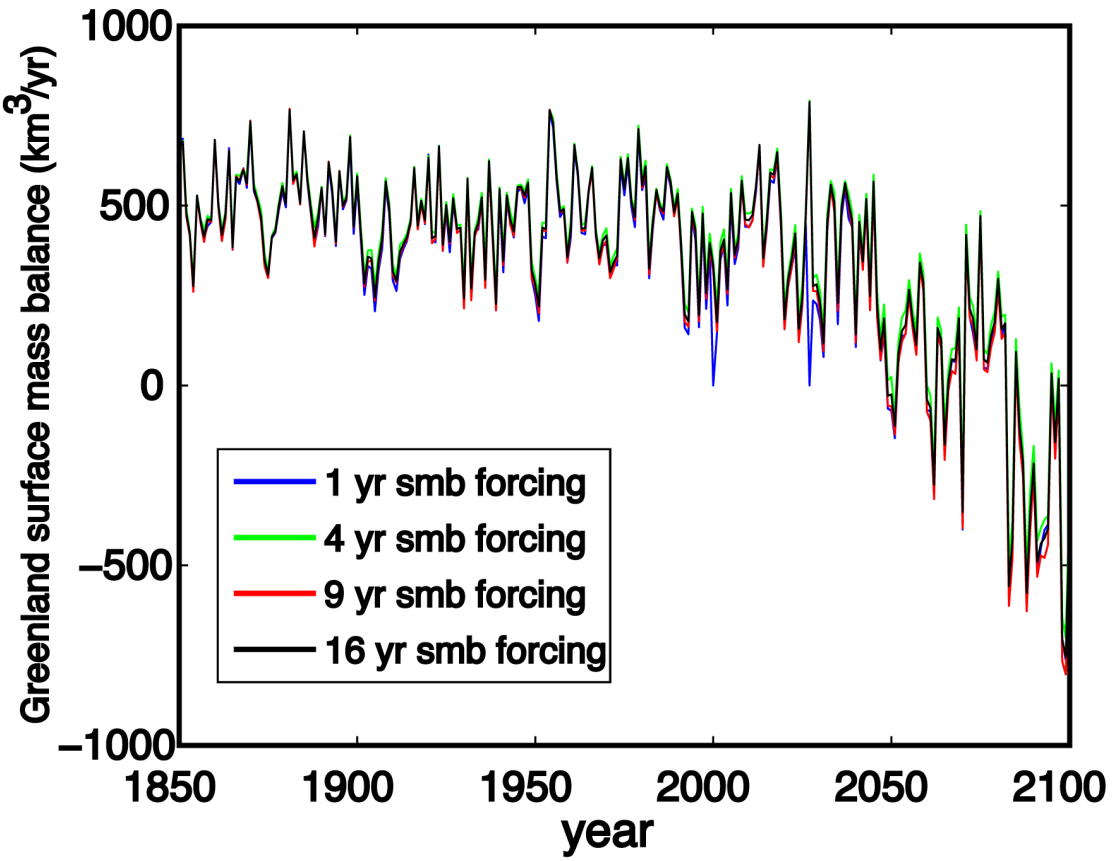

Figure 7: Ensemble mean Greenland Ice Sheet net surface mass balance evolution from 1850 to 2100. Despite variations in the initial state of the ice sheet for each experiment, the surface mass balance is similar across ensembles. Note that SMB declines over the entire time period, but rapidly becomes negative after 2005 when the RCP 8.5 emissions forcing is applied.

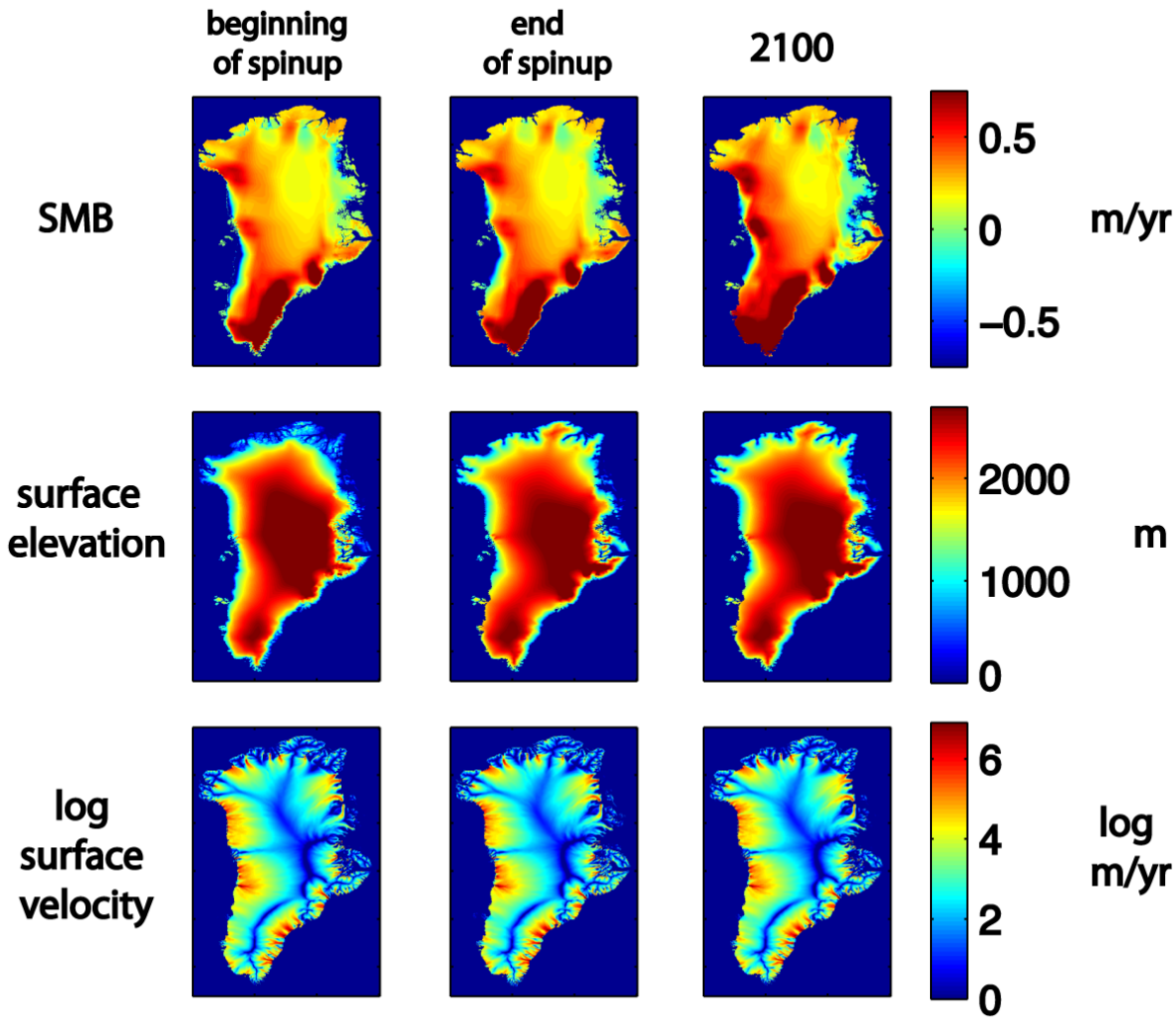

Figure 8: a) Surface mass balance, b) surface elevation, and c) log of surface velocity for the Greenland Ice Sheet. Columns correspond to values averaged over the first 400 years of spinup (left), averaged over the last 400 years of spinup (middle) and in year 2100 (right). Values correspond to ensemble means from the 4-year ensemble.

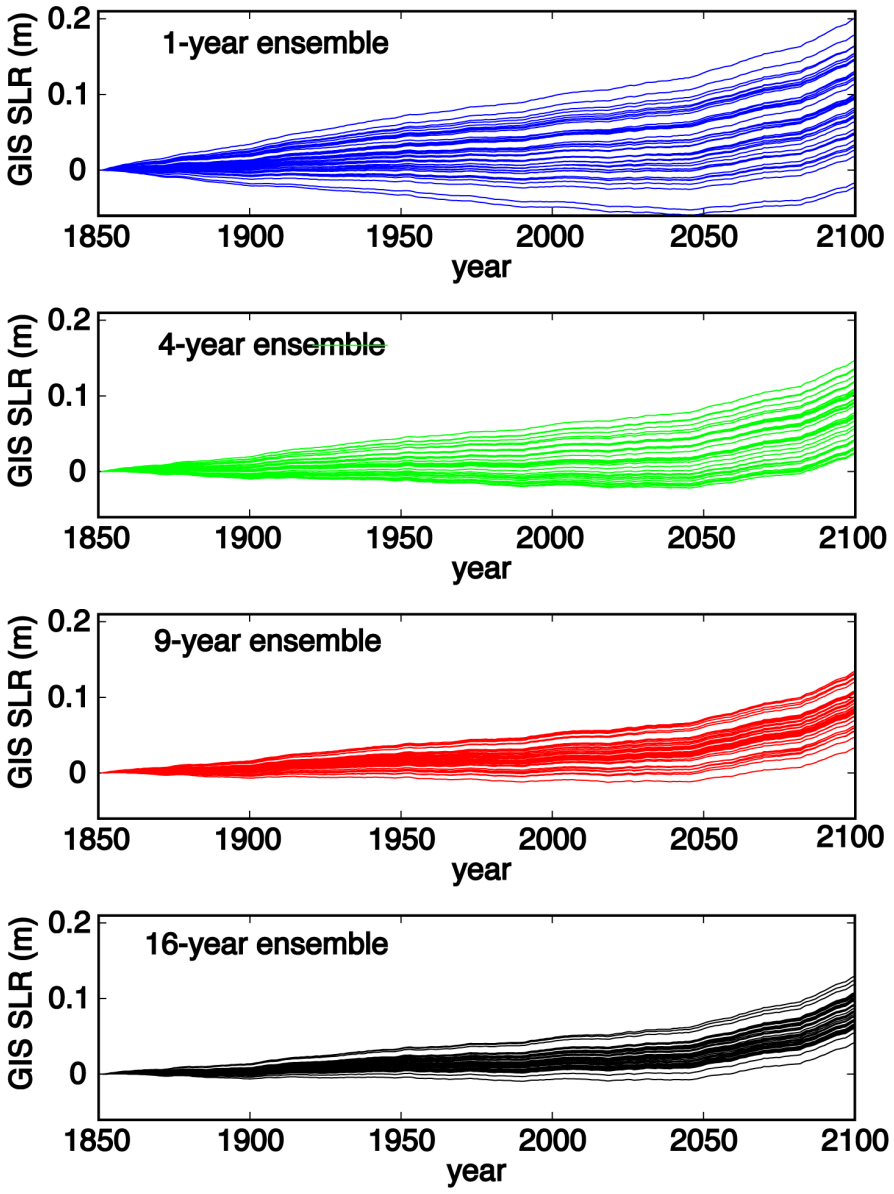

Figure 9: GIS SLR evolution for each experiment, separated by forcing ensemble. The 1-year ensemble demonstrates the most variability and includes model integrations that suggest a range of scenarios from a ~3 cm lowering in sea level to a 20 cm sea level rise by 2100. All integrations in the other three ensembles suggest a sea level rise between approximately 5 to10 cm between 1850 and 2100.

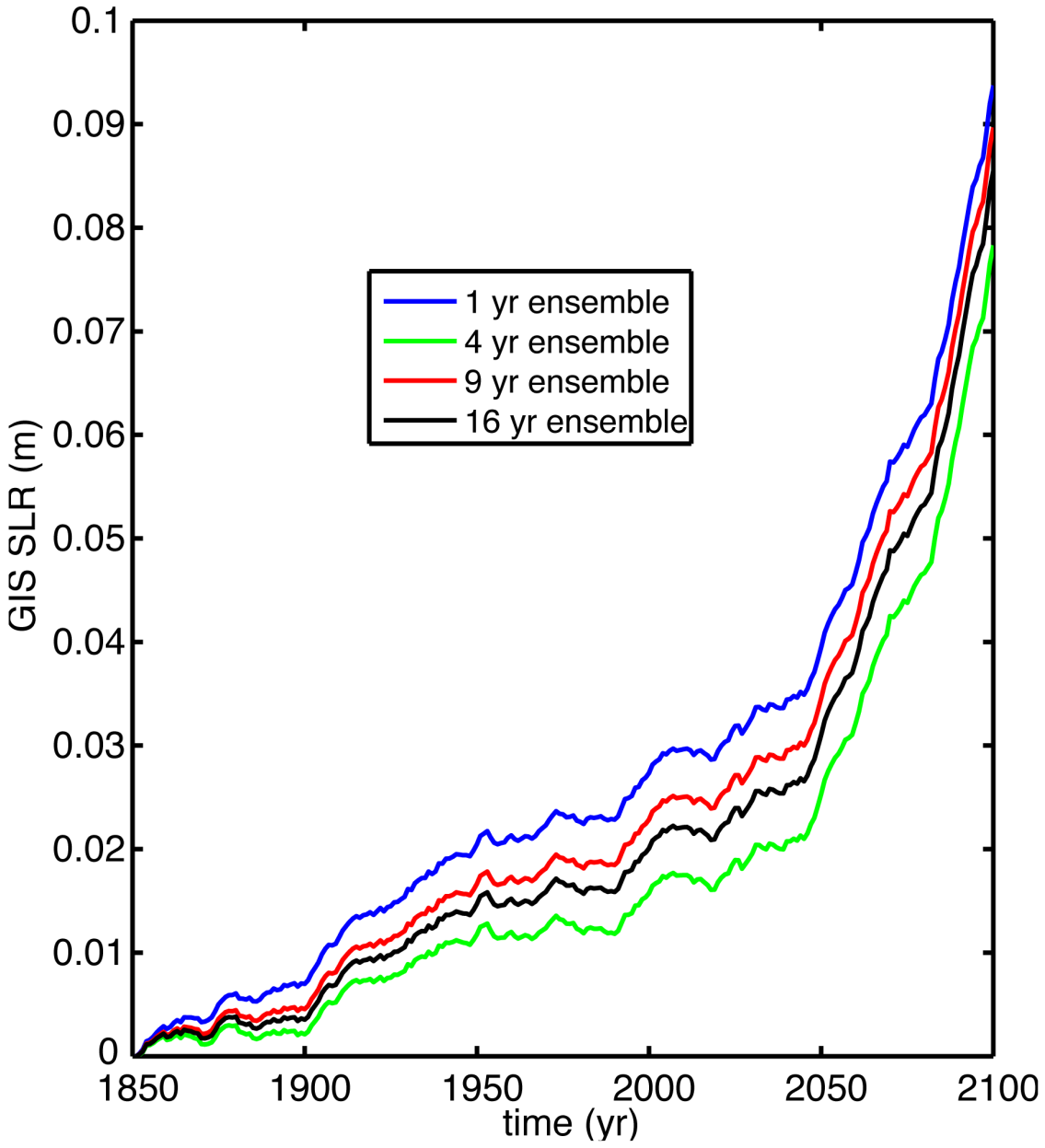

Figure 10: Greenland ice sheet contribution to sea level rise between 1850 and 2100. Each line shows the ensemble mean SLR. Between 1850 and 2050, the GIS is modeled to contribute approximately 0.25 mm/yr to global sea level on average. After 2050, the rate of GIS SLR increases to 1.2 mm/yr on average.

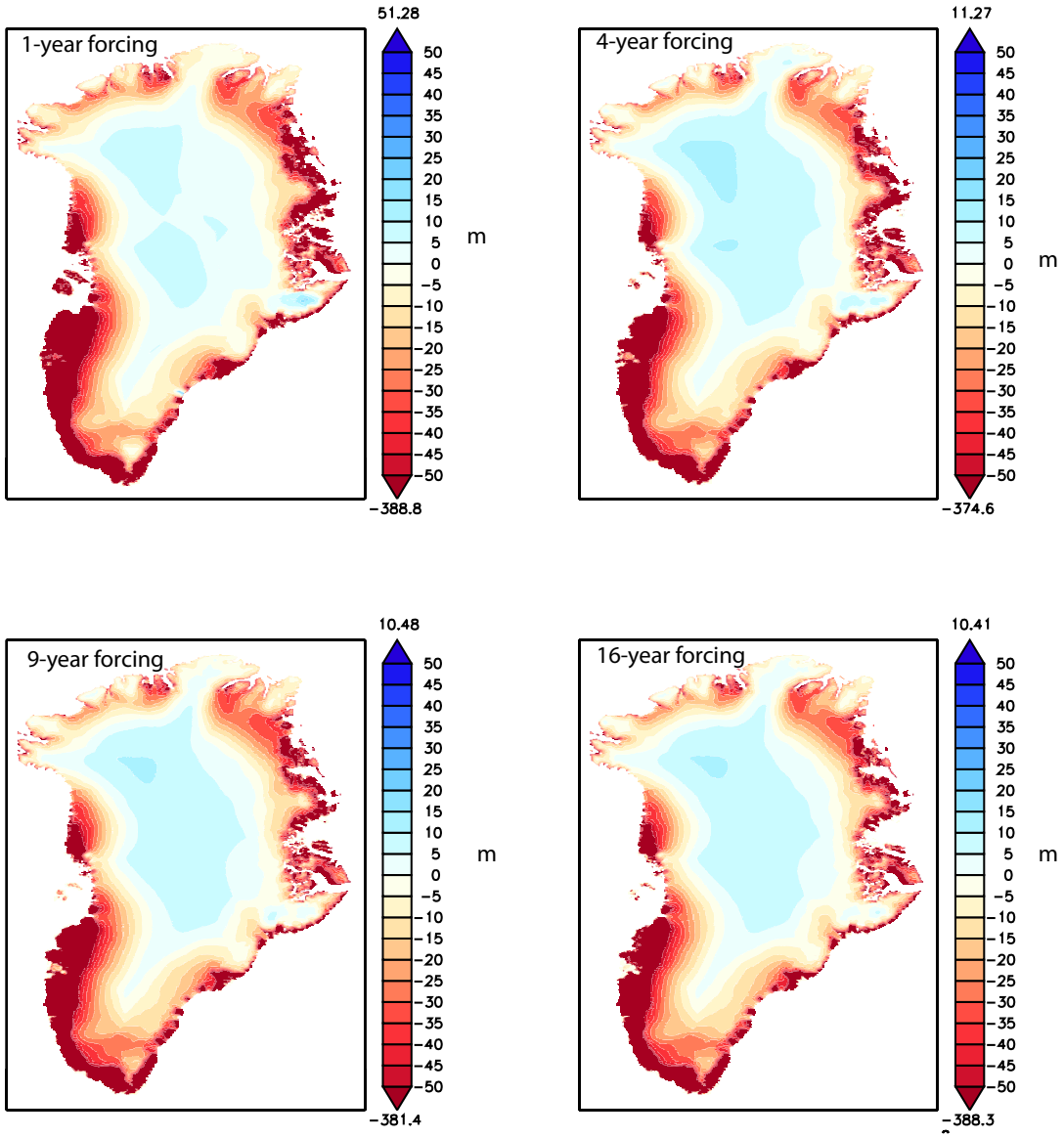

Figure 11: Mean change in ice thickness between 1850 and 2100 for each ensemble. All ensembles exhibit ~14% increase in ablation area in 2100 compared to 1850. This increase in ablating ice accounts for most of the ice sheet mass loss during our simulations.

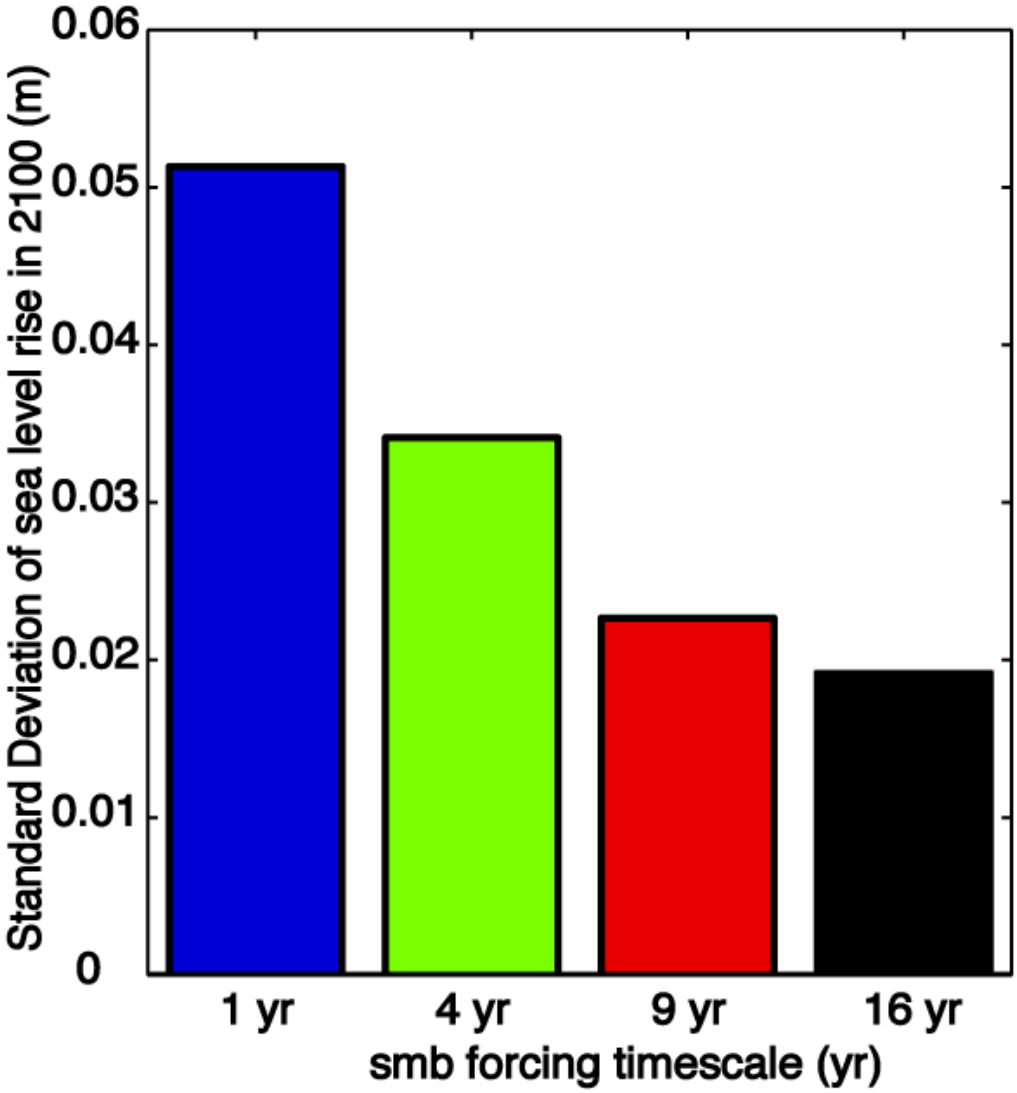

Figure 12: Standard deviation in 2100 sea level rise for each ensemble. As expected, uncertainty decreases as SMB forcing timescale increases due to a reduction in noise over longer timescales.

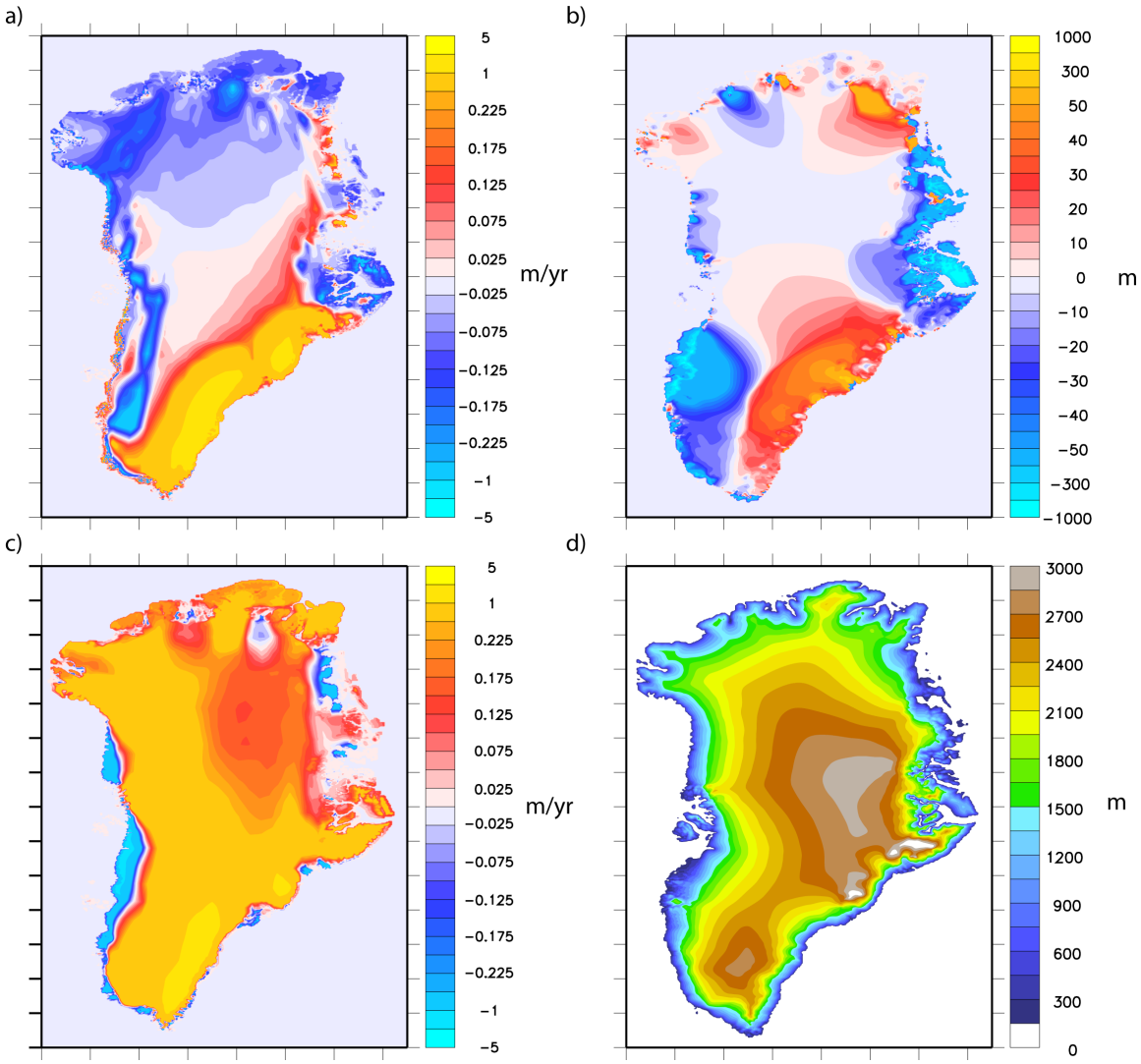

Figure 13: Feedbacks between SMB and surface elevation over the course of the spinup period for the full GIS. a) SMB anomaly at the beginning of spinup for ensemble member 20 over the full ice sheet; b) surface elevation anomaly at the end of the spinup; c) ensemble mean SMB at the beginning of the spinup; d) ensemble mean elevation at the end of the spinup. The southern areas of the ice sheet show positive SMB anomalies at the beginning of the spinup corresponding to positive surface elevation anomalies at the end of the spinup, as expected.

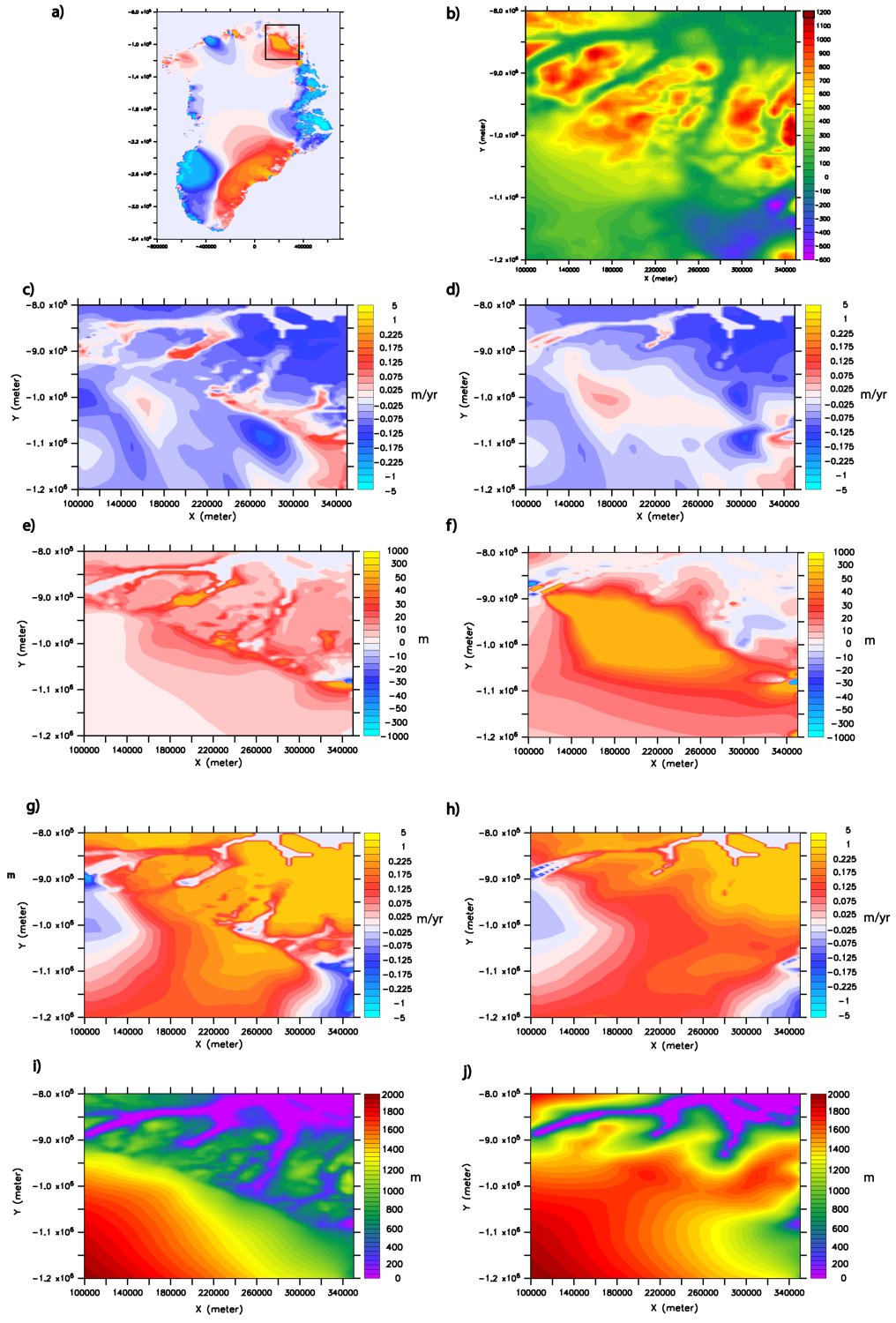
a)
b)
c)
d)
e)
f)
g)
h)
i)
j)
Y (meter)
X (meter)
m/yr
m

Figure 14: Example of a counterintuitive feedback along the northern margin of the GIS. a) rectangle showing the region where the feedback occurs; b) basal topography of the region demonstrating the location of valleys; c) SMB anomaly at the beginning of the spinup revealing anomalously high SMB in the valleys; d) SMB anomaly after the spinup; e) surface elevation anomaly at the beginning of the spinup; f) surface elevation anomaly at the end of the spinup. Figures g, h, i, and j depict mean values corresponding to Figures c, d, e, and f, respectively, included here for reference when interpreting anomalies. "Beginning of spinup" refers to an average over years 100 to 400, while "end of spinup" refers to an average over years 9600 to 9900 of the initialization period.

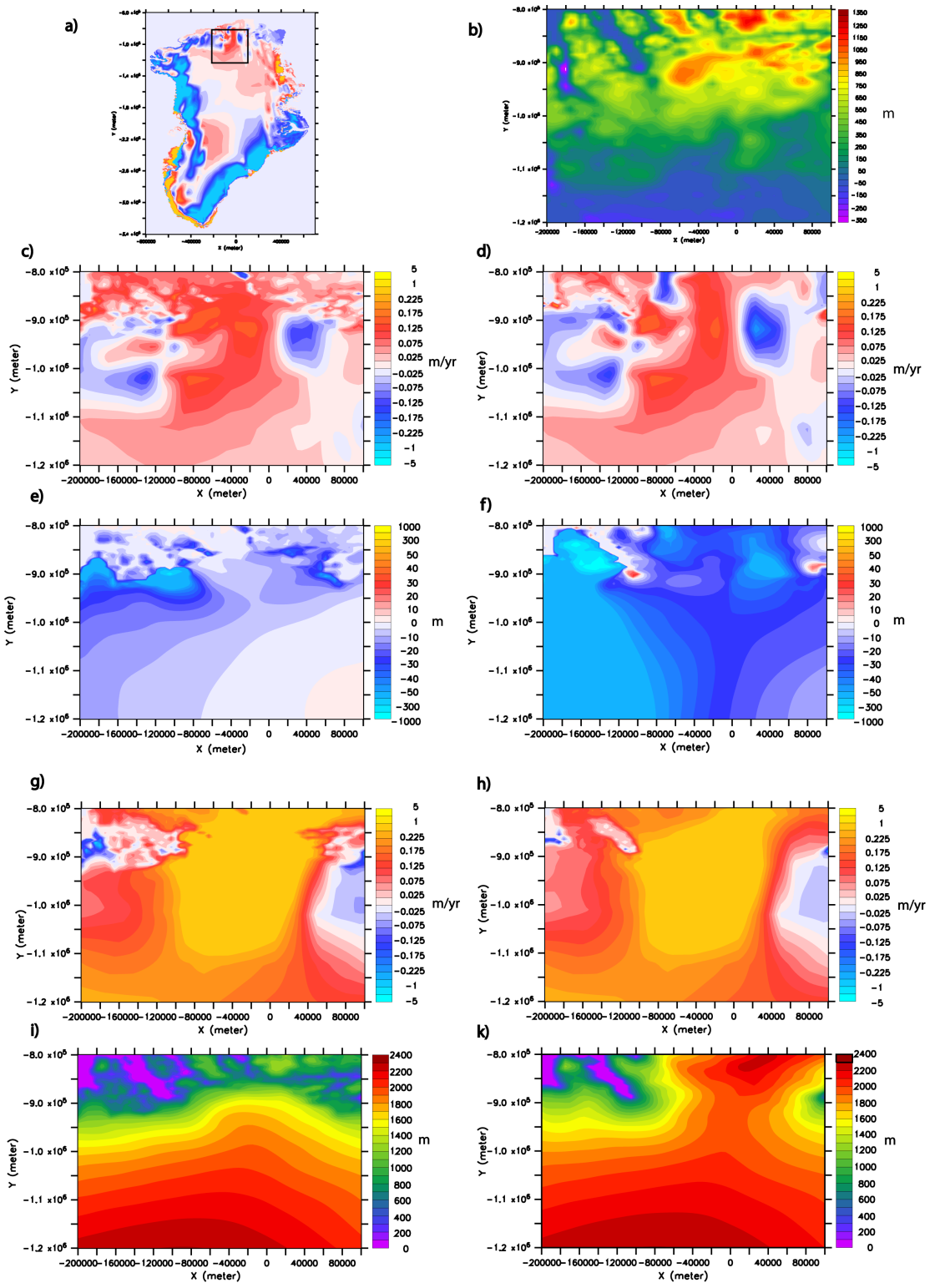
a)
b)
c)
d)
e)
f)
g)
h)
i)
k)
X (meter)
Y (meter)
m/yr
m

Figure 15: Alternate example of a counterintuitive feedback. a) rectangle showing the region where the feedback occurs; b) basal topography of the region; c) SMB anomaly at the beginning of the spinup; d) SMB anomaly after the spinup; e) surface elevation anomaly at the beginning of the spinup; f) surface elevation anomaly at the end of the spinup revealing a negative surface elevation anomaly despite the presence of a positive SMB anomaly at the end of the spinup.Figures g, h, i, and j depict mean values corresponding to Figures c, d, e, and f, respectively, included here for reference when interpreting anomalies. “Beginning of spinup” refers to an average over years 100 to 400, while “end of spinup” refers to an average over years 9600 to 9900 of the initialization period.

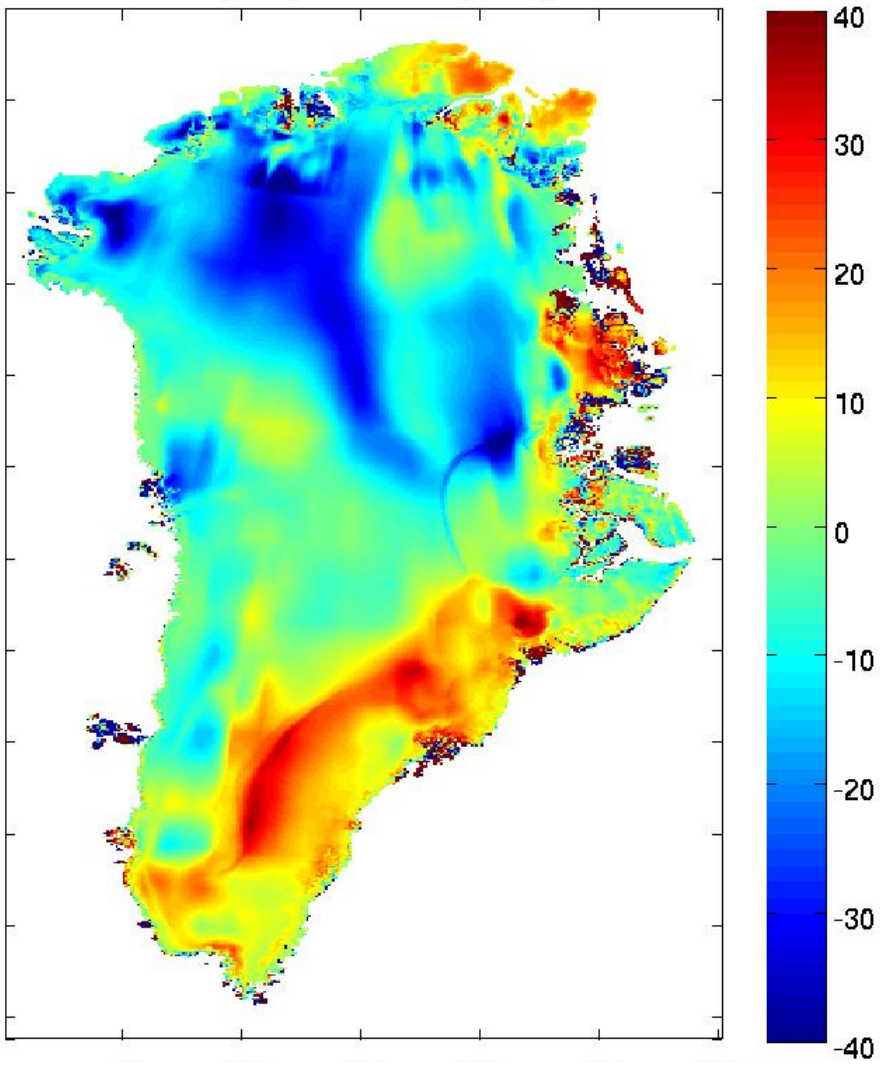

Figure 16: Sensitivity of elevation change (1850 to 2100) anomaly to SMB anomaly at the beginning of the spinup.

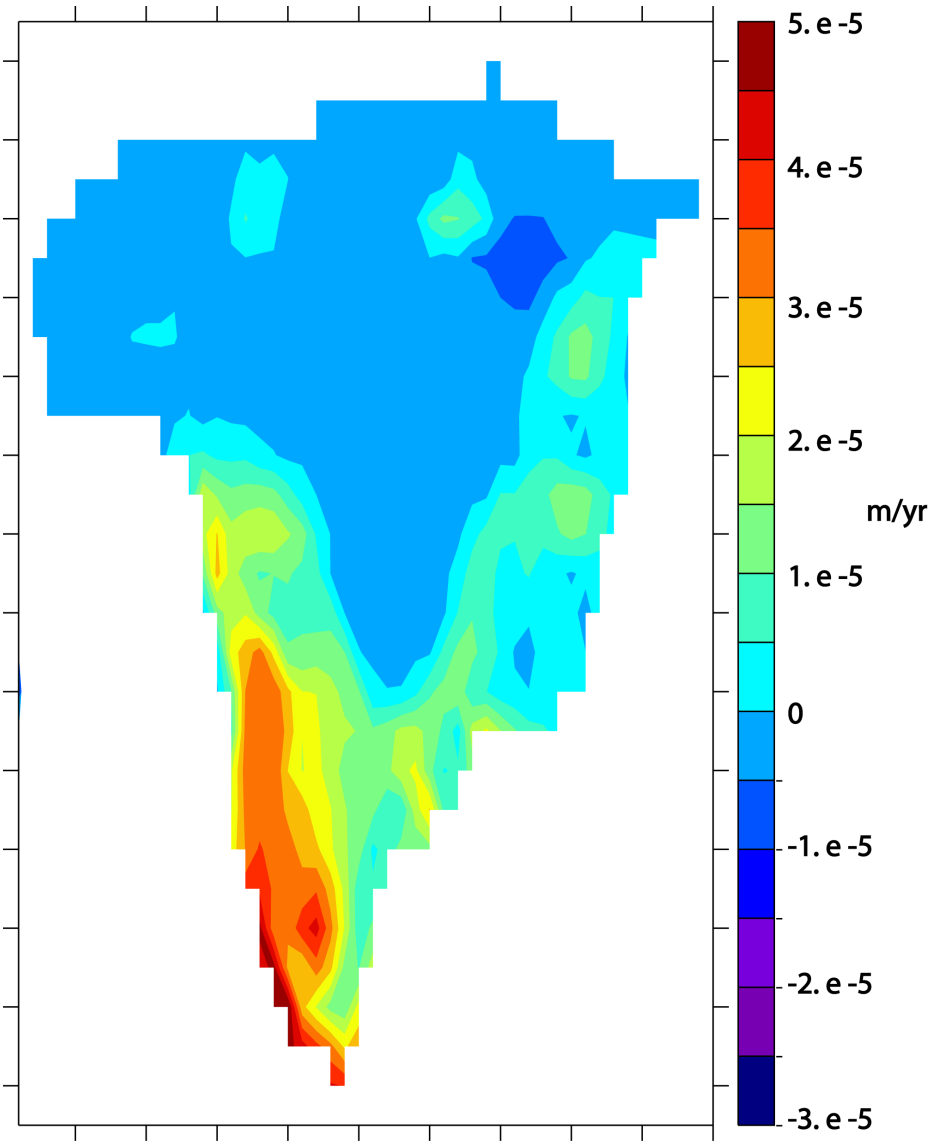

Figure 17: Vertical gradient of SMB between elevation classes 4 and 8, corresponding to elevations of 700 and 3000 m, respectively. There is an apparent difference in SMB as a function of elevation between the northern and southern parts of Greenland.

Tables

Options	Value	Description
temperature	1	Ice temperature solution: computed for whole ice column
flow_law	0	Ice flow law: Paterson-Budd temperature-dependent relationship
basal_water	2	No basal water included
marine_margin	1	Treatment of floating ice: set thickness to 0 if floating
slip_coeff	5	Basal traction parameter: constant where basal temp. is at pressure melting pt, otherwise no sliding
evolution	-1 for IG runs 0 for TG runs	Method of thickness evolution: turned off for SMB calculation (see Section 3.1); set to pseudo-diffusion for experiment runs
Sigma_levels	0.00 0.15 0.30 0.45 0.60 0.75 0.83 0.90 0.95 0.98 1.00	Vertical levels in sigma units, giving more resolution near the bed where shear is at a maximum
Parameters	**Value**	**Description**
dt	0.05	Ice sheet dynamic timestep: years between dynamic calls from the coupler to the ice sheet model
ntem	0.1	Temperature timestep in years
nvel	0.1	Velocity timestep in years
ice_limit	100	Thickness in meters below which ice dynamics are ignore
geothermal	0.061979	Geothermal heat flux in W/m2
flow_factor	2.7461	Correction to Glen's coefficient A, used to tune ice viscosity; greater values indicate lower viscosity
basal_tract	3.4158595068e-6 10 10 0 1	First value in this array is constant basal traction coefficient in m yr-1 Pa-1. Other values are not tunable.

Table 1: CISM parameters used to perform the model integrations in this study, except where noted in the text.

Forcing timescale	SLR, 1850 to 2100	SLR, 1850 to 2005	SLR, 2006 to 2100
1 year	9.4 ± 10.2 cm	2.9 cm	6.4 cm
4 years	7.8 ± 6.8 cm	1.7 cm	6.1 cm
9 years	9.0 ± 4.6 cm	2.5 cm	6.5 cm
16 years	8.6 ± 3.8 cm	2.2 cm	6.4 cm

Table 2: Modeled sea level rise for between 1850 and 2100 and for the 1850-2005 and 2006-2100, separately. In all model ensembles, sea level rise during the 21st century more than doubled compared to the 20th century sea level rise. Uncertainties expressed are 2σ significance.

Glossary

AIS: Antarctic Ice Sheet

CAM: Community Atmosphere Model

CESM: Community Earth System Model

CISM: Community Ice Sheet Model

CLM: Community Land Model

ECMWF: European Centre for Medium-Range Weather Forecasts

GCM: General Circulation Model

GIS: Greenland Ice Sheet

IPCC: Intergovernmental Panel on Climate Change

LWE: liquid water equivalent

PDD: Positive Degree Day

RACMO: Regional Atmospheric Climate Model

SLR: sea level rise

SMB: surface mass balance

Spinup: process of ice sheet model initialization, which ideally includes integrating model ice sheet until steady state is achieved

References

Bamber, J. L., R. L. Layberry and S. P. Gogineni (2001), A new ice thickness and bed data set for the Greenland ice sheet: 1. Measurement, data reduction, and errors. J. of Geophysical Research, 106(D24), 33773, doi:10.1029/2001JD900054.

Bamber, J.L., J.A. Griggs, R.T.W.L. Hurkmans, J.A. Dowdeswell, S.P. Goginenti, I. Howat, J. Mouginot, J. Paden, S. Palmer, E. Rignot and D. Steinhage (2011), A new bed elevation dataset for Greenland, The Cryosphere, 7, 499–510, doi:10.5194/tc-7-499-2013.

Bindschadler, R., S. Nowicki, A. Abe-Ouchi, A. Ashwanden, H. Choi, J. Fastook, G. Granzow, R. Greve, G. Gutowski, U. Herzfeld, C. Jackson, J. Johnson, C. Khroulev, A. Levermann, W. H. Lipscomb, M. A. Martin, M. Morlighem, B.R. Parizek, D. Pollard, S. F. Price, D. Ren, F. Saito, T. Sato, H. Seddik, H. Seroussi, H. Takahashi, R. Walker and W. L. Wang (2013), Ice-sheet model sensitivities to environmental forcing and their use in projecting future sea level (the SeaRISE project), J. of Glaciology, 59 (214).

Braithwaite, R. J. (1995), Positive degree-day factors for ablation on the Greenland ice sheet studied by energy-balance modelling. J. of Glaciology, 41(137), 1–8.

Church, J. A., & N.J. White (2006), A 20th century acceleration in global sea-level rise. Geophy. Res. Lett., 33(1), L01602. doi:10.1029/2005GL024826.

CReSIS (2010), Jakobshavn glacier elevation data. Tech. rep., Center for Remote Sensing of Ice Sheets. Ettema, J., M. R. van den Broeke, E. van Meijgaard, W. J. van de Berg, J. L. Bamber, J. E. Box and R. C. Bales (2009), Higher surface mass balance of the Greenland ice sheet revealed by high-resolution climate modeling, Geophys. Res. Lett., 36, L12501, doi:10.1029/2009GL038110.

Fettweis, X., B. Franco, M. Tedesco, J. H. van Angelen, J. T. M. Lenaerts, M. R. van den Broeke and H. Gallée (2013), Estimating the Greenland ice sheet surface mass balance contribution to future sea level rise using the regional atmospheric climate model MAR. The Cryosphere, 7(2), 469–489, doi:10.5194/tc-7-469-2013.

Fyke, J.G., A. Weaver, D. Pollard, M. Eby, L. Carter and A. Mackintosh (2011), A new coupled ice sheet/climate model: description and sensitivity to model physics under Eemian, Last Glacial Maximum, late Holocene and modern climate conditions. Geosci. Model Dev., 4, 117–136.

Hall, D. K., J. C. Comiso, N. E. DiGirolamo, C. A. Shuman, J. E. Box and L. S. Koenig (2013), Variability in the surface temperature and melt extent of the

Greenland ice sheet from MODIS, Geophys. Res. Lett., 40, 2114–2120, doi:10.1002/grl.50240.

IPCC (2007), Climate Change 2007: The Physical Science Basis. Contribution of Working Group I to the Fourth Assessment Report of the Intergovernmental Panel on Climate Change [Solomon, S., D. Qin, M. Manning, Z. Chen, M. Marquis, K.B. Averyt, M.Tignor and H.L. Miller (eds.)]. Cambridge University Press, Cambridge, United Kingdom and New York, NY, USA.

Larour, E., M. Morlighem and H. Seroussi (2012), Ice flow sensitivity to geothermal heat flux of Pine Island Glacier, Antarctica, J. of Geophysical Research, 117(F04023), doi:10.1029/2012JF002371.

Lipscomb, W.H. and W.J. Sacks (2012), The CESM Land Ice Model (CISM): Documentation and User's Guide.

Lipscomb, W. H., J. G. Fyke, M. Vizcaíno, W. J. Sacks, J. Wolfe, M. Vertenstein, A. Craig, E. Kluzek and D. Lawrence (2013), Implementation and initial evaluation of the Glimmer Communtiy Ice Sheet Model in the Community Earth System Model. J. of Climate, doi:10.1175/JCLI-D-12-005571.

Neale, R. B., A. Gettelman, S. Park, C. C. hen, P. H. Lauritzen, D. L. Williamson et al. (2011), Description of the NCAR Community Atmosphere Model (CAM 5.0). NCAR Technical note, 1–283.

Nicholls, R. J., and A. Cazenave (2010), Sea-Level Rise and Its Impact on Coastal Zones. Science, 328(5985), 1517–1520. doi:10.1126/science.1185782.

Oleson, K. et al. (2010), Technical Description of version 4.0 of the Community Land Model (CLM). Tech. rep., Climate and Global Dynamics Division, National Center for Atmospheric Research.

Paterson, W.S.B., and W.F. Budd (1982). Flow parameters for ice-sheet modeling. Cold Regions Sci. Techn. 6, 175-177.

Paul, F., A. Kääb, M. Maisch, T. Kellenberger, and W. Haeberli (2004), Rapid disintegration of Alpine glaciers observed with satellite data, Geophys. Res. Lett., 31, L21402, doi:10.1029/2004GL020816.

Payne, A.J. and D.J. Baldwin (2000), Analysis of ice-flow instabilities identified in the EISMINT intercomparison exercise, Ann. of Glaciology, 30(1), 204-210(7).

Pfeffer, W. T., J. T.Harper and S. O'Neel (2008), Kinematic constraints on glacier contributions to 21st-century sea-level rise. Science. 321(5894), 1340-1343, doi: 10.1126/science.1159099.

Pollard, D. (2000), Comparisons of ice-sheet surface mass budgets from Paleoclimate Modeling Intercomparison Project (PMIP) simulations. Glob. Plan. Change, 24 (2), 79–106, doi:10.1016/S0921-8181(99)00071-5.

Pritchard, M., A. Bush and S. Marshall (2008), Neglecting ice-atmosphere interactions underestimates ice sheet melt in millennial-scale deglaciation simulations. Geophys. Res. Lett., 35, doi:doi:10.1029/2007GL031738.

Rahmstorf, S. (2010), A new view on sea level rise. Nature Reports Climate Change, 44–45. doi:10.1038/climate.2010.29.

Rignot, E., I. Velicogna, M. Van Den Broeke, A. Monaghan, and J. Lenaerts (2011), Acceleration of the contribution of the Greenland and Antarctic ice sheets to sea level rise. Geophys. Res. Lett., 38, L05 503, doi:10.1029/2011GL046583.

Rutt, I., M. Hagdorn, N. Hulton, and A. Payne (2009), The Glimmer community ice sheet model. J. Geophys. Res., 114, doi:10.1029/2008JF001015.

Sriver, R. L., N. M. Urban, R. Olson and K. Keller (2012), Toward a physically plausible upper bound of sea-level rise projections. Climatic Change, 115(3-4), 893–902. doi:10.1007/s10584-012-0610-6.

van den Broeke, M., J. Bamber, J. Ettema, E. Rignot, E. Schrama, W.J. van der Berg, E. van Meijgaard, I. Velicogna, and B. Wouters (2009), Partitioning recent Greenland mass loss, Science, 326, 984-986.

Vizcaíno, M., W.H. Lipscomb, W.J. Sakcs, J.H. van Angelen, B. Wouters and M.R. van den Broeke (2013), Greenland Surface Mass Balance as Simulated by the Community Earth System Model. Part I: Model Evaluation and 1850-2005 Results. J. of Climate, doi:10.1175/JCLI-D-12-006151.